ASYMPTOTIC FIELDS AT FRICTIONLESS AND FRICTIONAL COHESIVE CRACK TIPS IN QUASIBRITTLE MATERIALS

QiZhi Xiao and Bhushan Lal Karihaloo

ASYMPTOTIC FIELDS AT FRICTIONLESS AND FRICTIONAL COHESIVE CRACK TIPS IN QUASIBRITTLE MATERIALS

QiZhi Xiao and Bhushan Lal Karihaloo

The lack of any work on the asymptotic fields at the tips of cohesive cracks belies the widespread use of cohesive crack models. This study is concerned with the solution of asymptotic fields at cohesive crack tips in quasibrittle materials. Only normal cohesive separation is considered, but the effect of Coulomb friction on the cohesive crack faces is studied. The special case of a pure mode I cohesive crack is fully investigated. The solution is valid for any separation law that can be expressed in a special polynomial form. It is shown that many commonly used separation laws of quasibrittle materials, for example, rectangular, linear, bilinear, and exponential, can be easily expressed in this form. The asymptotic fields obtained can be used as enrichment functions in the extended/generalized finite element method at the tip of long cohesive cracks, as well as short branches/kinks.

1. Introduction

Cohesive zone (or crack) models, which were introduced by Barenblatt [1962] and Dugdale [1960] for elastoplastic fracture in ductile metals, and by Hillerborg et al. [1976] for quasibrittle materials (who called them fictitious crack models), have become an important tool for describing localization and failure in engineering materials and structures. In a cohesive zone model, the nonlinear fracture process zone — due to degrading mechanisms such as plastic microvoiding or microcracking — in front of the actual crack tip is lumped into a discrete line (two-dimensional) or plane (three-dimensional) and represented by stress-displacement relationships across this line or plane. The cohesive crack model is a constitutive assumption in the sense that a cohesive crack can develop anywhere in a specimen or a structure, and not only ahead of a preexisting crack tip. For ductile fracture, the most important parameters of the cohesive zone model are the tensile strength f_t and the work of separation or fracture energy G_c (see, [Hutchinson and Evans 2000]), which is the work needed to create a unit area of a fully developed crack. For quasibrittle fracture, the decohesion law stems from microcracking as in concrete or ceramics; the shape of the stress-separation relation (called the softening or stress-crack opening or tension-softening curve) plays a much bigger role and is sometimes even more important than the value of the tensile strength f_t (see [Chandra et al. 2002]).

Elices et al. [2002] have reviewed the background of cohesive crack models and discussed the determination of the tension-softening function by inverse analysis procedures. They also illustrated the predictive capability of the cohesive zone model for concrete, glassy polymer and steel. Recently, Karihaloo et al. [2003] have proposed a simple method for determining the true specific fracture energy of concrete and also a method [Abdalla and Karihaloo 2004] for constructing a softening curve corresponding to this energy. In the most widely used standard formulation of the cohesive crack model for quasibrittle

materials, it is assumed that the stress-strain behavior is isotropic linear elastic, and that the crack is initiated at a point where the maximum principal stress σ_I reaches the tensile strength f_t, and that the crack is oriented normal to the direction of σ_I. An evolution law is also postulated for the monotonic mode I loading so that the cohesive stress is a unique function of the crack opening which, for concrete, decreases monotonically along the cohesive zone. Although this standard formulation of the cohesive crack model is highly simplified, it is able to capture the essence of fracture of concrete specimens and structures.

A concise overview of the various ways to implement numerically the cohesive zone methodology is given in [de Borst et al. 2004]. The recently developed extended/generalized finite element method (XFEM/GFEM) (see [Moës et al. 1999; Strouboulis et al. 2001; Babuška et al. 2003; Karihaloo and Xiao 2003b; Xiao and Karihaloo 2005]) provides a proper representation of the discrete character of cohesive zone formulations avoiding any mesh bias. The XFEM/GFEM enriches the standard local FE approximations with known information about the problem, such as a displacement discontinuity across a crack, the asymptotic solution at a crack tip, or a strain discontinuity across an interface, with the use of the partition of unity (PU). It avoids meshes conforming with the discontinuity and adaptive remeshing as the discontinuity grows as is the case with the FEM. Wells and Sluys [2001], Moës and Belytschko [2002] and Hansbo and Hansbo [2004] analyzed a continuous cohesive crack that runs through an existing FE mesh. Remmers et al. [2003] further studied the possibility of defining cohesive segments that can arise at arbitrary locations and in arbitrary directions and thus allow for the resolution of complex crack patterns including crack nucleation at multiple locations, followed by growth and coalescence. In these existing XFEM/GFEM implementations of the cohesive zone, the enrichment function used at the cohesive crack tip is usually a jump function (cohesive crack tip touches the element boundary) [Wells and Sluys 2001] or a branch function [Moës and Belytschko 2002] which does not represent the true asymptotic nature of the displacement/stress field there. (Hansbo and Hansbo [2004] considered an element traversed by a discontinuity as a double element with each being used for the interpolation of one side of the discontinuity). Recently, Xiao and Karihaloo [2005] have demonstrated that, for a crack with traction-free faces, when the crack tip asymptotic field is available and used as an enrichment function, the XFEM/GFEM not only avoids using a mesh conforming with the crack but is also more accurate than FEM. However, it is necessary to ensure that the unknown coefficients of the crack tip field at all the enriched nodes are equal to one another. Hence XFEM/GFEM can use a much coarser mesh around the crack tip. However, when the enrichment function does not represent the true asymptotic nature of the crack tip field, the mesh needs to be refined in the same manner as in the FEM. Thus it is advantageous to know the true asymptotic fields around a cohesive crack tip.

Planas et al. [2003] discussed possible generalizations of the cohesive crack model to mixed mode. Many other studies on mixed mode cohesive cracks can also be found in the literature, for example, [Valente 1991; Cocchetti et al. 2002], but there is doubt about the accuracy of the cohesion-sliding relation because it is difficult to isolate it from frictional forces between the rough cohesive crack faces in quasibrittle materials such as concrete.

Coulomb friction along the contacting crack faces has been considered by many researchers. Deng [1994] studied the plane strain/stress asymptotic crack tip fields of stationary and steadily moving cracks along bimaterial interfaces and in homogeneous solids. He considered both anisotropic and isotropic solids. Leblond and Frelat [2004] studied crack kinking from an initially closed, homogeneous or

interface crack, in the presence of Coulomb friction. Bialas and Mróz [2005] analyzed progressive interface delamination failure in antiplane shear of an elastic plate bonded to a rigid substrate under monotonic loading by normal compressive stress and varying shear stress using the cohesive crack model. Mróz and Bialas [2005] considered a rigid softening interface (critical stress softening) under both monotonic and cyclic loadings.

In the cohesive cracks, the friction is considered for a finite opening. In this sense frictional cohesive cracks are different from the previously mentioned works on frictional contact of crack faces, where the crack faces are in contact and not open. However, in cohesive cracks, although the crack faces are not in contact because of the applied cohesive stresses, frictional forces can come into play between the faces when there is relative sliding.

Hong and Kim [2003] studied plane elastic eigenfunction expansions of the cohesive crack tip field due to the closing tractions and the separation-gradients at the cohesive zone ahead of a semiinfinite crack in an inverse manner, similar to that used by Karihaloo [1999]. In these works, the softening curve is not defined a priori but is obtained parametrically from the analysis. This often leads to softening diagrams that are not representative of real materials [Planas et al. 2001].

The lack of any work on the asymptotic fields at the tips of cohesive cracks belies the widespread use of cohesive crack models. In this study, we will solve the asymptotic fields at the tips of cohesive cracks in quasibrittle materials. The material outside the fracture process (that is, cohesive) zone is isotropic linear elastic. This is true of quasibrittle materials. We will consider frictionless as well as frictional cohesive cracks. We will use the eigenfunction expansion method of Williams [1957] and combine it with the complex function formalism of Muskhelishvili [1953] in the spirit of Sih and Liebowitz [1968]. The cohesive and frictional laws on the crack faces are imposed through appropriate boundary conditions.

This paper is organized as follows: Section 2 discusses a cohesive law of concrete suitable for the asymptotic analysis of cohesive cracks; Section 3 discusses the mathematical formulation and local symmetry and/or boundary conditions; Section 4 gives asymptotic fields for several cases; Section 5 discusses the applicability of the results obtained in Section 4 to other cohesive laws; the implementation of the asymptotic fields in XFEM/GFEM is illustrated in Section 6 with examples of mode I cohesive crack tip fields; and finally conclusions and discussion are presented in Section 7.

2. Reformulation of a tension-softening diagram for quasibrittle materials

Cornelissen et al. [1986] introduced the following exponential relation to fit their results from uniaxial tests on double edge notched normal and lightweight concrete panels:

$$\frac{\sigma}{f_t} = f\left(\frac{w}{w_c}\right) - \frac{w}{w_c} f(1), \qquad f\left(\frac{w}{w_c}\right) = \left[1 + \left(C_1 \frac{w}{w_c}\right)^3\right] e^{-C_2 w/w_c}. \tag{1}$$

It fits their experimental results with a high degree of accuracy. In Equation (1), σ and f_t are the stress normal to the cohesive crack face and the uniaxial tensile strength, respectively; w and w_c are the opening displacement of the cohesive crack faces, and the critical opening displacement of the preexisting macrocrack tip at which the cohesive crack tip begins to grow; and C_1 and C_2 are fitting parameters. Details of the test set up as well as the cohesive relation Equation (1) can be found in [Karihaloo 1995].
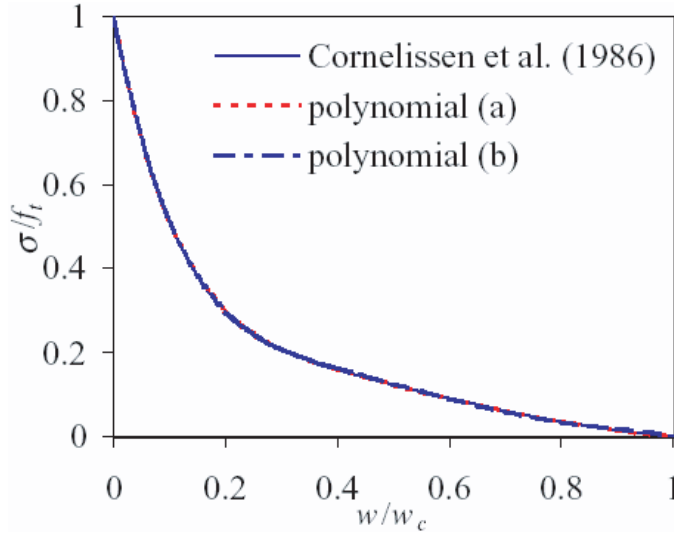
Figure 1. A comparison of formula Equation (1) with polynomials (2) and (3) for NC.

The following polynomial, denoted as polynomial (a), fits the results of Cornelissen et al. [1986] just as well as Equation (1)

$$\frac{\sigma}{f_t} = 1 + \sum_{i=1}^{5} a_i \left(\frac{w}{w_c}\right)^i - \left(1 + \sum_{i=1}^{5} a_i\right)\left(\frac{w}{w_c}\right)^6, \tag{2}$$

where the a_i, $i = 1, \ldots, 5$, are fitting parameters.

To simplify the derivation of the cohesive crack tip asymptotic fields, we will represent the relation Equation (1) by the polynomial, denoted polynomial (b),

$$\frac{\sigma}{f_t} = 1 + \sum_{i=1}^{5} \alpha_i \left(\frac{w}{w_c}\right)^{(2/3)i} - \left(1 + \sum_{i=1}^{5} \alpha_i\right)\left(\frac{w}{w_c}\right)^4, \tag{3}$$

where the α_i, $i = 1, \ldots, 5$, are fitting parameters.

Obviously, all three formulae (1)–(3) satisfy the following requirements: at the tip of the cohesive crack, $w/w_c = 0$ and $\sigma/f_t = 1$; at the tip of the preexisting traction-free macrocrack: if $w/w_c = 1$ then $\sigma/f_t = 0$.

Note that although there are five unknown parameters in (2) and (3) to be determined by regression, this is easier than the determination of the two parameters in the exponential relation (1).

For a normal concrete (NC) with density $2370 \, \text{kg/m}^3$, compressive strength $f_c = 47 \, \text{MPa}$, Young modulus $E = 39 \, \text{GPa}$, $f_t = 3.2 \, \text{MPa}$, $w_c = 160 \, \mu\text{m}$, and specific fracture energy $G_F = 100 \, \text{J/m}^2$ (area under the tension-softening curve), Cornelissen et al. [1986] fitted their experimental results by Equation (1) with $C_1 = 3$ and $C_2 = 6.93$. Their tension-softening diagram can be fitted by Equation (2) with $a_1 = -7.04$, $a_2 = 26.456$, $a_3 = -55.233$, $a_4 = 63.741$, and $a_5 = -38.305$. The correlation coefficient is 1. This diagram can also be fitted by Equation (3) with $\alpha_1 = -0.872$, $\alpha_2 = -16.729$, $\alpha_3 = 67.818$,
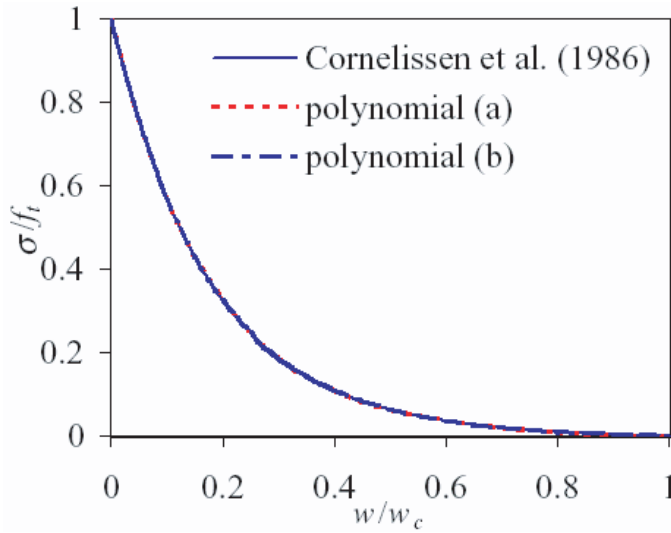
Figure 2. A comparison of formula Equation (1) with polynomials (2) and (3) for LC.

$\alpha_4 = -110.462$, and $\alpha_5 = 83.158$. The correlation coefficient is again 1. These three fittings are compared in Figure 1, and cannot be distinguished on the scale of the figure.

For a lightweight concrete (LC) with density 1865 kg/m^3, $f_c = 49$ MPa, $E = 22.4$ GPa, $f_t = 2.43$ MPa, $w_c = 140\,\mu$m, and $G_F = 61$ J/m^2, Cornelissen et al. [1986] fitted their experimental results by Equation (1) with $C_1 = 1$ and $C_2 = 5.64$. Their tension-softening diagram can be fitted by Equation (2) with $a_1 = -5.618$, $a_2 = 15.36$, $a_3 = -25.378$, $a_4 = 25.659$ and $a_5 = -14.525$. The correlation coefficient is 1. This diagram can also be fitted by polynomial Equation (3) with $\alpha_1 = -0.753$, $\alpha_2 = -12.335$, $\alpha_3 = 41.08$, $\alpha_4 = -57.205$, and $\alpha_5 = 38.412$. The correlation coefficient is again 1. These three fittings are compared in Figure 2, and again cannot be distinguished on the scale of the figure.

3. Mathematical formulation

Muskhelishvili [1953] showed that, for plane problems, the stresses and displacements in the Cartesian coordinate system (see Figure 3) can be expressed in terms of two analytic functions $\phi(z)$ and $\chi(z)$ of the complex variable $z = re^{i\theta}$

$$
\begin{aligned}
\sigma_x + \sigma_y &= 2\big[\phi'(z) + \overline{\phi'(z)}\,\big], \\
\sigma_y - \sigma_x + 2i\,\tau_{xy} &= 2\big[\bar{z}\phi''(z) + \chi''(z)\big], \\
2\mu(u + iv) &= \kappa\phi(z) - z\overline{\phi'(z)} - \overline{\chi'(z)},
\end{aligned}
\tag{4}
$$

where a prime denotes differentiation with respect to z, and an overbar denotes a complex conjugate. In Equation (4), $\mu = E/[2(1 + \nu)]$ is the shear modulus; the Kolosov constant is $\kappa = 3 - 4\nu$ for plane strain or $\kappa = (3 - \nu)/(1 + \nu)$ for plane stress; E and ν are Young's modulus and the Poisson ratio.

For a general plane mixed mode I + II problem, the complex functions $\phi(z)$ and $\chi(z)$ can be chosen as series of complex eigenvalue Goursat functions [Sih and Liebowitz 1968; Owen and Fawkes 1983;
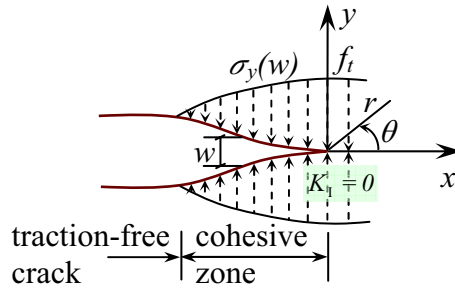
Figure 3. A real traction-free crack terminating in a fracture process (cohesive) zone (FPZ) with residual stress transfer capacity $\sigma_y(w)$ whose faces close smoothly near its tip ($K_1 = 0$). The material outside the FPZ is linear elastic, but within the FPZ is softening.

Karihaloo and Xiao 2003a]

$$
\begin{aligned}
\phi(z) &= \sum_{n=0} A_n z^{\lambda_n} && = \sum_{n=0} A_n r^{\lambda_n} e^{i\lambda_n\theta}, \\
\chi(z) &= \sum_{n=0} B_n z^{\lambda_n+1} = \sum_{n=0} B_n r^{\lambda_n+1} e^{i(\lambda_n+1)\theta},
\end{aligned}
\tag{5}
$$

where the complex coefficients are $A_n = a_{1n} + ia_{2n}$ and $B_n = b_{1n} + ib_{2n}$. The eigenvalues λ_n and coefficients a_{1n}, a_{2n}, b_{1n} and b_{2n} are real.

If we substitute the complex functions Equation (5) into (4), the complete series expansions of the displacements and stresses near the tip of the crack become

$$
2\mu u = \sum_{n=0} r^{\lambda_n} \Big\{ \kappa(a_{1n}\cos\lambda_n\theta - a_{2n}\sin\lambda_n\theta) + \lambda_n\big[-a_{1n}\cos(\lambda_n-2)\theta + a_{2n}\sin(\lambda_n-2)\theta\big] \\
+ (\lambda_n+1)(-b_{1n}\cos\lambda_n\theta + b_{2n}\sin\lambda_n\theta)\Big\},
\tag{6}
$$

$$
2\mu v = \sum_{n=0} r^{\lambda_n} \Big\{ \kappa(a_{1n}\sin\lambda_n\theta + a_{2n}\cos\lambda_n\theta) + \lambda_n\big[a_{1n}\sin(\lambda_n-2)\theta + a_{2n}\cos(\lambda_n-2)\theta\big] \\
+ (\lambda_n+1)(b_{1n}\sin\lambda_n\theta + b_{2n}\cos\lambda_n\theta)\Big\},
\tag{7}
$$

$$
\sigma_x = \sum_{n=0} r^{\lambda_n-1} \Big\{ 2\lambda_n\big[a_{1n}\cos(\lambda_n-1)\theta - a_{2n}\sin(\lambda_n-1)\theta\big] \\
- \lambda_n(\lambda_n-1)\big[a_{1n}\cos(\lambda_n-3)\theta - a_{2n}\sin(\lambda_n-3)\theta\big] \\
- (\lambda_n+1)\lambda_n\big[b_{1n}\cos(\lambda_n-1)\theta - b_{2n}\sin(\lambda_n-1)\theta\big]\Big\},
\tag{8}
$$

$$
\sigma_y = \sum_{n=0} r^{\lambda_n-1} \Big\{ 2\lambda_n\big[a_{1n}\cos(\lambda_n-1)\theta - a_{2n}\sin(\lambda_n-1)\theta\big] \\
+ \lambda_n(\lambda_n-1)\big[a_{1n}\cos(\lambda_n-3)\theta - a_{2n}\sin(\lambda_n-3)\theta\big] \\
+ (\lambda_n+1)\lambda_n\big[b_{1n}\cos(\lambda_n-1)\theta - b_{2n}\sin(\lambda_n-1)\theta\big]\Big\},
\tag{9}
$$

$$\tau_{xy} = \sum_{n=0} r^{\lambda_n-1} \Big\{ \lambda_n(\lambda_n - 1)\big[a_{1n} \sin(\lambda_n - 3)\theta + a_{2n} \cos(\lambda_n - 3)\theta\big]$$
$$+ (\lambda_n + 1)\lambda_n\big[b_{1n} \sin(\lambda_n - 1)\theta + b_{2n} \cos(\lambda_n - 1)\theta\big]\Big\}. \quad (10)$$

The opening displacement (COD) behind the cohesive zone tip is

$$w = v\big|_{\theta=\pi} - v\big|_{\theta=-\pi} = \sum_{n=0} \frac{r^{\lambda_n}}{\mu}\big[(\kappa + \lambda_n)a_{1n} + (\lambda_n + 1)b_{1n}\big] \sin \lambda_n \pi \quad (11)$$

and the sliding displacement of the crack faces is

$$\delta = u\big|_{\theta=\pi} - u\big|_{\theta=-\pi} = \sum_{n=0} \frac{r^{\lambda_n}}{\mu}\big[(\lambda_n - \kappa)a_{2n} + (\lambda_n + 1)b_{2n}\big] \sin \lambda_n \pi. \quad (12)$$

To complete the asymptotic analysis of the crack tip fields, solutions need to satisfy the proper symmetry conditions along the line of extension of the cohesive crack, and boundary conditions on the cohesive crack faces.

If the crack faces are traction-free (that is, there is no cohesive zone), then

$$\sigma_y\big|_{\theta=\pi} = \sigma_y\big|_{\theta=-\pi} = 0, \qquad \tau_{xy}\big|_{\theta=\pi} = \tau_{xy}\big|_{\theta=-\pi} = 0. \quad (13)$$

If normal cohesive separation applies to the crack faces, relationship Equation (3) needs to be satisfied over the cohesive zone. The stresses at the cohesive crack tip are nonsingular (because the stress intensity factor $K_I = 0$). Moreover, the following conditions need to be satisfied:

(a) If the cohesive crack faces are frictionless, we have

$$\sigma_y\big|_{\theta=\pi} = \sigma_y\big|_{\theta=-\pi} \neq 0, \qquad \tau_{xy}\big|_{\theta=\pi} = \tau_{xy}\big|_{\theta=-\pi} = 0, \quad (14)$$

(b) If the Coulomb friction is considered, we have

$$\sigma_y\big|_{\theta=\pi} = \sigma_y\big|_{\theta=-\pi} \neq 0, \qquad \tau_{xy}\big|_{\theta=\pi} = \tau_{xy}\big|_{\theta=-\pi} = -\mu_f \sigma_y\big|_{\theta=\pm\pi} \neq 0, \quad (15)$$

where μ_f equals the positive or negative value of the coefficient of kinetic friction, which is assumed to be constant, depending on the relative sliding direction of the two crack faces. Specifically, $\mu_f > 0$ when $\delta > 0$ and $\mu_f < 0$ when $\delta < 0$.

(c) If the cohesive crack faces are in pure mode I condition, we have

$$\sigma_y\big|_{\theta=\pi} = \sigma_y\big|_{\theta=-\pi} \neq 0, \quad \tau_{xy}\big|_{\theta=\pi} = \tau_{xy}\big|_{\theta=-\pi} = 0, \quad \tau_{xy}\big|_{\theta=0} = 0, \quad v\big|_{\theta=0} = 0. \quad (16)$$

In all three situations, the length of the process (cohesive) zone is either prescribed (that is, an initial cohesive zone exists before the loading is applied, and does not propagate under the present loading) or is determined by the condition $w = w_c$ in the normal cohesion-separation relation Equation (3) at the instant of growth of the preexisting traction-free crack.

4. Asymptotic crack tip fields

For completeness and later use, we will first deduce the Williams expansion for a traction-free crack without a cohesive zone.

4.1. *Williams expansions for cracks with traction-free faces.* After enforcing the traction-free conditions Equation (13) on the crack faces, we have

$$\lambda_n = \tfrac{1}{2}n, \ n = 0, 1, 2, \ldots \tag{17}$$

and

$$-b_{1n} = \frac{(n/2) + (-1)^n}{(n/2) + 1} a_{1n}, \qquad -b_{2n} = \frac{(n/2) - (-1)^n}{(n/2) + 1} a_{2n}. \tag{18}$$

It is easy to confirm that with the eigenvalues Equation (17) and the coefficient relationships (18) the solutions (6)–(10) reduce to the well-known Williams expansions [Owen and Fawkes 1983; Karihaloo and Xiao 2003a]:

$$u = \sum_{n=0}^{\infty} \frac{r^{n/2}}{2\mu} \left\{ a_{1n}\left[\left(\kappa + \tfrac{1}{2}n + (-1)^n\right) \cos\tfrac{1}{2}n\theta - \tfrac{1}{2}n \cos\left(\tfrac{1}{2}n - 2\right)\theta \right] \right.$$
$$\left. - a_{2n}\left[\left(\kappa + \tfrac{1}{2}n - (-1)^n\right) \sin\tfrac{1}{2}n\theta - \tfrac{1}{2}n \sin\left(\tfrac{1}{2}n - 2\right)\theta \right] \right\}, \quad (19)$$

$$v = \sum_{n=0}^{\infty} \frac{r^{n/2}}{2\mu} \left\{ a_{1n}\left[\left(\kappa - \tfrac{1}{2}n - (-1)^n\right) \sin\tfrac{1}{2}n\theta + \tfrac{1}{2}n \sin\left(\tfrac{1}{2}n - 2\right)\theta \right] \right.$$
$$\left. + a_{2n}\left[\left(\kappa - \tfrac{1}{2}n + (-1)^n\right) \cos\tfrac{1}{2}n\theta + \tfrac{1}{2}n \cos\left(\tfrac{1}{2}n - 2\right)\theta \right] \right\}, \quad (20)$$

$$\sigma_x = \sum_{n=1}^{\infty} \tfrac{1}{2}n\, r^{(n/2)-1} \left\{ a_{1n}\left[\left(2 + \tfrac{1}{2}n + (-1)^n\right) \cos\left(\tfrac{1}{2}n - 1\right)\theta - \left(\tfrac{1}{2}n - 1\right) \cos\left(\tfrac{1}{2}n - 3\right)\theta \right] \right.$$
$$\left. - a_{2n}\left[\left(2 + \tfrac{1}{2}n - (-1)^n\right) \sin\left(\tfrac{1}{2}n - 1\right)\theta - \left(\tfrac{1}{2}n - 1\right) \sin\left(\tfrac{1}{2}n - 3\right)\theta \right] \right\}, \quad (21)$$

$$\sigma_y = \sum_{n=1}^{\infty} \tfrac{1}{2}n\, r^{(n/2)-1} \left\{ a_{1n}\left[\left(2 - \tfrac{1}{2}n - (-1)^n\right) \cos\left(\tfrac{1}{2}n - 1\right)\theta + \left(\tfrac{1}{2}n - 1\right) \cos\left(\tfrac{1}{2}n - 3\right)\theta \right] \right.$$
$$\left. - a_{2n}\left[\left(2 - \tfrac{1}{2}n + (-1)^n\right) \sin\left(\tfrac{1}{2}n - 1\right)\theta + \left(\tfrac{1}{2}n - 1\right) \sin\left(\tfrac{1}{2}n - 3\right)\theta \right] \right\}, \quad (22)$$

$$\tau_{xy} = \sum_{n=1}^{\infty} \tfrac{1}{2}n\, r^{(n/2)-1} \left\{ a_{1n}\left[\left(\tfrac{1}{2}n - 1\right) \sin\left(\tfrac{1}{2}n - 3\right)\theta - \left(\tfrac{1}{2}n + (-1)^n\right) \sin\left(\tfrac{1}{2}n - 1\right)\theta \right] \right.$$
$$\left. + a_{2n}\left[\left(\tfrac{1}{2}n - 1\right) \cos\left(\tfrac{1}{2}n - 3\right)\theta - \left(\tfrac{1}{2}n - (-1)^n\right) \cos\left(\tfrac{1}{2}n - 1\right)\theta \right] \right\}. \quad (23)$$

The displacements corresponding to $n = 0$

$$u_0 = \frac{\kappa + 1}{2\mu} a_{10}, \qquad v_0 = \frac{\kappa + 1}{2\mu} a_{20} \tag{24}$$

are rigid body translations at the crack tip. The displacements corresponding to a_{22}

$$\hat{u}_2 = -\frac{\kappa + 1}{2\mu} a_{22}r \sin\theta = -\frac{\kappa + 1}{2\mu} a_{22}y,$$
$$\hat{v}_2 = \frac{\kappa + 1}{2\mu} a_{22}r \cos\theta = \frac{\kappa + 1}{2\mu} a_{22}x \tag{25}$$

represent the rigid body rotation $\theta_0 = -(\kappa + 1)a_{22}/(2\mu)$ with respect to the crack tip, with $x = r\cos\theta$ and $y = r\sin\theta$. Terms involving a_{10}, a_{20} and a_{22} do not contribute to the strains or stresses. Terms involving coefficients a_{1n} (a_{2n}), $n \geq 1$, correspond to pure mode I (II) expansions. The corresponding opening and sliding displacements of the crack faces are

$$w = \sum_{n=1,3,5,\ldots} \frac{r^{n/2}}{\mu} a_{1n}(\kappa + 1)\sin(n\pi/2) \tag{26}$$

$$\delta = \sum_{n=1,3,5,\ldots} -\frac{r^{n/2}}{\mu} a_{2n}(\kappa + 1)\sin(n\pi/2). \tag{27}$$

4.2. Frictionless cohesive crack with normal cohesive separation. The relationship Equation (3) between cohesion and normal separation will be discussed below after considering conditions Equation (14) on the crack faces.

Imposition of the left side of Equation (14) on (9) gives

$$(a_{2n} + b_{2n})\sin(\lambda_n - 1)\pi = 0 \implies \begin{cases} \lambda_n = n + 1, \quad \text{for } n = 0, 1, 2, \ldots \quad \text{(a)} \\ \text{or} \\ b_{2n} = -a_{2n} \quad\quad\quad\quad\quad\quad\quad\quad \text{(b)} \end{cases}$$

and imposition of the right side of Equation (14) on (10) gives

$$\left[(\lambda_n - 1)a_{1n} + (\lambda_n + 1)b_{1n}\right]\sin(\lambda_n - 1)\pi = 0$$
$$\left[(\lambda_n - 1)a_{2n} + (\lambda_n + 1)b_{2n}\right]\cos(\lambda_n - 1)\pi = 0.$$

We thus have for case (a)

$$b_{2n} = -\frac{\lambda_n - 1}{\lambda_n + 1}a_{2n},$$

and for case (b)

$$\cos(\lambda_n - 1)\pi = 0, \quad \text{or equivalently,} \quad \lambda_n = \frac{2n + 1}{2} + 1 \text{ for } n = 0, 1, 2, \ldots$$

and

$$b_{1n} = -\frac{\lambda_n - 1}{\lambda_n + 1}a_{1n}.$$

Taken together, the solutions are composed of two parts. The first part corresponds to integer eigenvalues

$$\text{(a)} \quad \lambda_n = n + 1, \qquad b_{2n} = -\frac{n}{n + 2}a_{2n}, \qquad n = 0, 1, 2, \ldots, \tag{28}$$

giving

$$\sigma_y\big|_{\theta = \pm\pi} = \sum_{n=0}(n + 2)(n + 1)r^n(a_{1n} + b_{1n})\cos n\pi$$

or

$$\hat{\sigma}_y = \frac{\sigma_y|_{\theta = \pm\pi}}{f_t} = \sum_{n=0} c_n r^n = 1 + \sum_{n=1} c_n r^n, \tag{29}$$

where

$$c_n = \frac{(n+2)(n+1)(a_{1n}+b_{1n})\cos n\pi}{f_t} \quad \text{and} \quad c_0 = \frac{2(a_{10}+b_{10})}{f_t} = 1, \tag{30}$$

since $\sigma_y|_{\theta=\pm\pi} = f_t$ when $r \to 0$.

The opening and sliding displacements of the cohesive crack faces vanish for integer eigenvalues

$$w = 0 \quad \text{and} \quad \delta = 0. \tag{31}$$

The second part of the asymptotic solutions corresponds to noninteger eigenvalues

$$\text{(b)} \ \lambda_n = \frac{2n+3}{2}, \qquad b_{1n} = -\frac{2n+1}{2n+5}a_{1n}, \qquad b_{2n} = -a_{2n}, \ n = 0, 1, 2, \ldots, \tag{32}$$

giving

$$\sigma_y|_{\theta=\pm\pi} = 0,$$

$$w = \sum_{n=0}^{\infty} \frac{r^{(2n+3)/2}}{\mu}\left[\left(\kappa + \frac{2n+3}{2}\right)a_{1n} + \frac{2n+5}{2}b_{1n}\right]\sin\frac{2n+3}{2}\pi \tag{33}$$

or

$$\hat{w} = \frac{w}{w_c} = \sum_{n=0}^{\infty} \bar{d}_n r^{(2n+3)/2},$$

$$\bar{d}_n = \frac{\left[(\kappa + (2n+3)/2)a_{1n} + ((2n+5)/2)b_{1n}\right]\sin((2n+3)/2)\pi}{\mu w_c}, \tag{34}$$

$$\delta = \sum_{n=0}^{\infty} \frac{r^{(2n+3)/2}}{\mu}\left[\left(\frac{2n+3}{2} - \kappa\right)a_{2n} + \frac{2n+5}{2}b_{2n}\right]\sin\frac{2n+3}{2}\pi. \tag{35}$$

The cohesive separation relationship Equation (3) is rewritten in normalized form using (29) and (34):

$$\hat{\sigma}_y = 1 + \sum_{i=1}^{5} \alpha_i \hat{w}^{(2/3)i} - \left(1 + \sum_{i=1}^{5} \alpha_i\right)\hat{w}^4. \tag{36}$$

Consider the truncated $N + 1$ terms of $\hat{w}$ Equation (34), and set $d_0 = \bar{d}_0$, $d_n = \bar{d}_n/d_0$ for $n > 1$. We have

$$\hat{w} = d_0 r^{3/2}\left(1 + \sum_{n=1}^{N} d_n r^n\right). \tag{37}$$

The expansion of $\hat{w}$ raised to the power $(2/3)i$ is also truncated to $N + 1$ terms, since these terms include only the truncated $N + 1$ terms of $\hat{w}$. Hence

$$\hat{w}^{(2/3)i} = d_0^{(2/3)i} r^i \left(1 + \sum_{n=1}^{N} \beta_{in} r^n\right) \tag{38}$$

with

$$\beta_{in} = \frac{f_i^{(n)}(0)}{n!}, \qquad f_i(r) = \left(1 + \sum_{n=1}^{N} d_n r^n\right)^{(2/3)i}, \tag{39}$$

where $f_i^{(n)}(0)$ denotes the n-th derivative at $r = 0$.

The first five derivatives of $f_i(r)$ Equation (39) are given in the Appendix, and the corresponding five coefficients β_{in} are

$$\beta_{i1} = \tfrac{2}{3}id_1,$$

$$\beta_{i2} = \tfrac{1}{3}i\left(\tfrac{2}{3}i - 1\right)d_1^2 + \tfrac{2}{3}id_2,$$

$$\beta_{i3} = \tfrac{1}{9}i\left(\tfrac{2}{3}i - 1\right)\left(\tfrac{2}{3}i - 2\right)d_1^3 + \tfrac{2}{3}i\left(\tfrac{2}{3}i - 1\right)d_1d_2 + \tfrac{2}{3}id_3,$$

$$\beta_{i4} = \tfrac{1}{36}i\left(\tfrac{2}{3}i - 1\right)\left(\tfrac{2}{3}i - 2\right)\left(\tfrac{2}{3}i - 3\right)d_1^4 + \tfrac{1}{3}i\left(\tfrac{2}{3}i - 1\right)\left(\tfrac{2}{3}i - 2\right)d_1^2d_2$$
$$+ \tfrac{1}{3}i\left(\tfrac{2}{3}i - 1\right)d_2^2 + \tfrac{2}{3}i\left(\tfrac{2}{3}i - 1\right)d_1d_3 + \tfrac{2}{3}id_4, \tag{40}$$

$$\beta_{i5} = \tfrac{1}{180}i\left(\tfrac{2}{3}i - 1\right)\left(\tfrac{2}{3}i - 2\right)\left(\tfrac{2}{3}i - 3\right)\left(\tfrac{2}{3}i - 4\right)d_1^5,$$
$$+ \tfrac{1}{9}i\left(\tfrac{2}{3}i - 1\right)\left(\tfrac{2}{3}i - 2\right)\left(\tfrac{2}{3}i - 3\right)d_1^3d_2$$
$$+ \tfrac{1}{3}i\left(\tfrac{2}{3}i - 1\right)\left(\tfrac{2}{3}i - 2\right)d_1d_2^2 + \tfrac{1}{3}i\left(\tfrac{2}{3}i - 1\right)\left(\tfrac{2}{3}i - 2\right)d_1^2d_3$$
$$+ \tfrac{2}{3}i\left(\tfrac{2}{3}i - 1\right)d_2d_3 + \tfrac{2}{3}i\left(\tfrac{2}{3}i - 1\right)d_1d_4 + \tfrac{2}{3}id_5.$$

With the use of Equation (38), the right hand side of the cohesive relationship (36) becomes

$$1 + \sum_{i=1}^{5} \alpha_i d_0^{(2/3)i} r^i \left(1 + \sum_{n=1}^{N} \beta_{in} r^n\right) - \left(1 + \sum_{i=1}^{5} \alpha_i\right) d_0^4 r^6 \left(1 + \sum_{n=1}^{N} \beta_{6n} r^n\right).$$

If we choose $N = 5$, then after satisfying the cohesive relationship Equation (36) we have the following expressions for the coefficients c_n in Equation (29):

$$c_1 = \alpha_1 d_0^{2/3},$$

$$c_2 = \alpha_2 d_0^{4/3} + \alpha_1 d_0^{2/3}\beta_{11},$$

$$c_3 = \alpha_3 d_0^2 + \alpha_1 d_0^{2/3}\beta_{12} + \alpha_2 d_0^{4/3}\beta_{21},$$

$$c_4 = \alpha_4 d_0^{8/3} + \alpha_1 d_0^{2/3}\beta_{13} + \alpha_2 d_0^{4/3}\beta_{22} + \alpha_3 d_0^2\beta_{31},$$

$$c_5 = \alpha_5 d_0^{10/3} + \alpha_1 d_0^{2/3}\beta_{14} + \alpha_2 d_0^{4/3}\beta_{23} + \alpha_3 d_0^2\beta_{32} + \alpha_4 d_0^{8/3}\beta_{41},$$

$$c_6 = \alpha_1 d_0^{2/3}\beta_{15} + \alpha_2 d_0^{4/3}\beta_{24} + \alpha_3 d_0^2\beta_{33} + \alpha_4 d_0^{8/3}\beta_{42} + \alpha_5 d_0^{10/3}\beta_{51} - \left(1 + \sum_{i=1}^{5}\alpha_i\right)d_0^4,$$

$$c_7 = \alpha_2 d_0^{4/3}\beta_{25} + \alpha_3 d_0^2\beta_{34} + \alpha_4 d_0^{8/3}\beta_{43} + \alpha_5 d_0^{10/3}\beta_{52} - \left(1 + \sum_{i=1}^{5}\alpha_i\right)d_0^4\beta_{61},$$

$$c_8 = \alpha_3 d_0^2\beta_{35} + \alpha_4 d_0^{8/3}\beta_{44} + \alpha_5 d_0^{10/3}\beta_{53} - \left(1 + \sum_{i=1}^{5}\alpha_i\right)d_0^4\beta_{62},$$

$$c_9 = \alpha_4 d_0^{8/3}\beta_{45} + \alpha_5 d_0^{10/3}\beta_{54} - \left(1 + \sum_{i=1}^{5}\alpha_i\right)d_0^4\beta_{63},$$

$$c_{10} = \alpha_5 d_0^{10/3}\beta_{55} - \left(1 + \sum_{i=1}^{5}\alpha_i\right)d_0^4\beta_{64},$$

$$c_{11} = -\left(1 + \sum_{i=1}^{5}\alpha_i\right)d_0^4\beta_{65}. \tag{41}$$

The asymptotic solution above is not for a pure mode I cohesive crack tip (compare Equation (14) and (16)), since along the line of extension of the crack, $\theta = 0$, the shear stress does not vanish ($\tau_{xy} \neq 0$).

For noninteger eigenvalues Equation (39), the coefficients a_{1n} and a_{2n} may be regarded as independent, so that coefficients b_{1n} are linearly dependent on a_{1n} and b_{2n} on a_{2n}. For integer eigenvalues (28), coefficients a_{1n} and a_{2n} may also be regarded as independent, so that coefficients b_{2n} now depend linearly on a_{2n}. However, the coefficients b_{1n} for integer eigenvalues will depend both linearly on a_{1n} for integer eigenvalues and nonlinearly on a_{1n} for noninteger eigenvalues via (37), (34), (37), (39) and (41). The inherent nonlinear nature of the problem is reflected in these nonlinear relationships between the coefficients of the asymptotic fields.

The displacements (8), (7) corresponding to $\lambda_{-1} = 0$, or $n = -1$ in (35) are rigid body translations at the crack tip

$$2\mu u_{-1} = \kappa a_{1,-1} - b_{1,-1}, \qquad 2\mu v_{-1} = \kappa a_{2,-1} + b_{2,-1}. \tag{42}$$

The displacements corresponding to a_{20} ($n = 0$, $\lambda_0 = 1$ and $b_{20} = 0$ from Equation (28)) represent rigid body rotation with respect to the crack tip

$$2\mu \hat{u}_0 = -r(\kappa + 1)a_{20}\sin\theta, \qquad 2\mu \hat{v}_0 = r(\kappa + 1)a_{20}\cos\theta. \tag{43}$$

4.3. _Coulomb frictional cohesive crack with normal cohesive separation._ In principle, a cohesive relationship can also be considered in the tangential direction for quasibrittle materials. However, this is a contentious issue, since it is difficult to separate the cohesive-sliding relation from the frictional force between the rough cohesive crack faces. Hence, in the following, we consider the Coulomb friction between the crack faces instead of a tangential cohesive relationship. The corresponding boundary conditions are Equation (15).

The complete asymptotic solutions are again composed of two parts. The first part corresponding to integer eigenvalues is similar to case (a) in Section 4.2 but with different constraints on the coefficients

$$\lambda_n = n + 1, \qquad na_{2n} + (n+2)b_{2n} = -\mu_f(n+2)(a_{1n} + b_{1n}), \ n = 0, 1, 2, \ldots. \tag{44}$$

From (44), we have

$$b_{2n} = -\frac{n}{n+2}a_{2n} - \mu_f(a_{1n} + b_{1n}).$$

When $\mu_f = 0$, the cohesive crack faces are frictionless, and Equation (44) reduces to (28). These solutions have nonzero σ_y and τ_{xy} along the cohesive crack faces, but zero crack opening w. The second part of the asymptotic solutions corresponding to noninteger eigenvalues satisfies

$$b_{1n} = -\frac{\lambda_n - 1}{\lambda_n + 1}a_{1n}, \qquad b_{2n} = -a_{2n}, \quad (\mu_f a_{1n} - a_{2n})\cos(\lambda_n - 1)\pi = 0. \tag{45}$$

If we assume that

$$\mu_f a_{1n} - a_{2n} \neq 0, \tag{46}$$

the third equation in Equation (45) gives

$$\cos(\lambda_n - 1)\pi = 0 \tag{47}$$

so that the second part of asymptotic solutions is identical to (b) of Section 4.2 (that is, (33)–(35)).

The remaining solution procedure and final asymptotic solutions as well as the dependence of the coefficients are similar to those in 4.2. Equations (42) and (43) again represent the rigid body modes for the present case.

4.4. *A pure mode I cohesive crack.*

For a pure mode I cohesive crack, the crack faces are frictionless. After satisfying the conditions (16)$_3$ and (16)$_4$, we have

$$
\begin{aligned}
(\lambda_n - 1)a_{2n} + (\lambda_n + 1)b_{2n} &= 0 \\
(\kappa + \lambda_n)a_{2n} + (\lambda_n + 1)b_{2n} &= 0
\end{aligned}
\tag{48}
$$

and finally $a_{2n} = b_{2n} = 0$. Conditions (16)$_1$ and (16)$_2$ are satisfied if $[(\lambda_n - 1)a_{1n} + (\lambda_n + 1)b_{1n}] \sin(\lambda_n - 1)\pi$ vanishes, which is to say,

$$
\begin{cases}
\lambda_n = n + 1, n = 0, 1, 2, \ldots & \text{(c)} \\
\text{or} \\
b_{1n} = -\dfrac{\lambda_n - 1}{\lambda_n + 1} a_{1n}. & \text{(d)}
\end{cases}
$$

Solution (c) gives the same normal cohesive stress σ_y as Equation (29) along the cohesive crack faces and a nonvanishing σ_y along the line of extension of the crack, but without a jump in the normal displacement w, that is, as in Equation (31).

Solution (d) corresponds to noninteger eigenvalues. Without loss of generality, but to simplify the enforcement of the normal cohesive relationship Equation (36), we can choose such noninteger eigenvalues that result in no tractions on the cohesive crack faces (but a nonvanishing σ_y along the line of extension of the crack) and a displacement discontinuity w in the normal direction. In other words,

$$
\sigma_y\big|_{\theta=\pm\pi} = 0 \Rightarrow (a_{1n} + b_{1n}) \cos(\lambda_n - 1)\pi = 0 \Rightarrow \lambda_n = \frac{2n + 3}{2}, \ n = 0, 1, 2, \ldots.
\tag{49}
$$

It is easy to confirm that these solutions are nothing but the nonsingular odd terms in pure mode I Williams expansions Equation (19)–Equation (23) for a traction-free crack:

$$
u = \sum_{n=1} \frac{r^{(2n+1)/2}}{2\mu} a_{1n} \left[\left(\kappa + \frac{2n-1}{2} \right) \cos \frac{2n+1}{2}\theta - \frac{2n+1}{2} \cos \frac{2n-3}{2}\theta \right]
\tag{50}
$$

$$
v = \sum_{n=1} \frac{r^{(2n+1)/2}}{2\mu} a_{1n} \left[\left(\kappa - \frac{2n-1}{2} \right) \sin \frac{2n+1}{2}\theta + \frac{2n+1}{2} \sin \frac{2n-3}{2}\theta \right]
\tag{51}
$$

$$
\sigma_x = \sum_{n=1} \frac{2n+1}{2} r^{(2n-1)/2} a_{1n} \left(\frac{2n+3}{2} \cos \frac{2n-1}{2}\theta - \frac{2n-1}{2} \cos \frac{2n-5}{2}\theta \right)
\tag{52}
$$

$$
\sigma_y = \sum_{n=1} \frac{2n+1}{2} r^{(2n-1)/2} a_{1n} \left(\frac{-2n+5}{2} \cos \frac{2n-1}{2}\theta + \frac{2n-1}{2} \cos \frac{2n-5}{2}\theta \right)
\tag{53}
$$

$$
\tau_{xy} = \sum_{n=1} \frac{2n+1}{2} r^{(2n-1)/2} a_{1n} \left(\frac{2n-1}{2} \sin \frac{2n-5}{2}\theta - \frac{2n-1}{2} \sin \frac{2n-1}{2}\theta \right).
\tag{54}
$$

Solutions (c) and (d) together give the asymptotic solutions for a pure mode I cohesive crack. The normal cohesive relationship is satisfied in the same way as in Section 4.2. The COD corresponding to Equation (51) is

$$
w = \sum_{n=0} \frac{r^{(2n+3)/2}}{\mu} a_{1n}(\kappa + 1) \sin \frac{2n+3}{2}\pi
$$

$$
\hat{w} = \sum_{n=0} \bar{d}_n r^{(2n+3)/2}, \qquad \bar{d}_n = \frac{(\kappa + 1)}{\mu w_c} a_{1n} \sin \frac{2n+3}{2}\pi.
$$

(55)

Now $\hat{w}$ can again be reformulated as Equation (37), but the coefficients d_n are different. For the cohesive law Equation (36), the formal relationships between the coefficients will be the same as Equation (41).

Note that the rigid body modes for the present case are no longer represented by Equation (42) and Equation (43), but are

$$
u_{\text{rigid}} = u_0 + y\theta_0 = u_0 + \theta_0 r \sin\theta,
$$

$$
v_{\text{rigid}} = v_0 - x\theta_0 = v_0 - \theta_0 r \cos\theta.
$$

(56)

These rigid body modes must be appended to the asymptotic fields above to obtain the complete crack tip displacements. However, in the analysis of pure mode I crack problems, it is more efficient to use symmetry conditions along the line of extension of the crack, and set $u_0 = v_0 = \theta_0 = 0$.

5. Applicability of the results to other cohesive-separation diagrams

From the formulation in Section 4, it became clear that the eigenvalues and asymptotic fields are uniquely defined for traction-free cracks (Section 4.1) and frictionless cohesive cracks with normal cohesion between their faces (Section 4.2). However, for a crack with normal cohesion and Coulomb friction (Section 4.3), and a pure mode I cohesive crack (Section 4.4), the eigenvalues and asymptotic fields are not completely unique. Additional assumptions had to be made to ensure uniqueness. Thus, in Section 4.3 we imposed the additional condition Equation (46) and in Section 4.4 the condition (49). These conditions however do not lead to any loss of generality.

The derivations above were for a special form of the normal cohesion-separation relation (3), or equivalently, (36), which made the expansion of a power of $\hat{w}$ in (37) possible, as shown in (38). Since this relation has five free parameters, it is believed to be able to fit a large amount of experimental data on many grades of concrete. It was already shown above to represent almost exactly the exponential relation (1). Below we show that it can equally accurately represent other normal cohesion-separation relations commonly used for quasibrittle materials.

The widely used linear tension-softening law

$$
\hat{\sigma}_y = 1 - \hat{w}
$$

(57)

cannot be used in the previous asymptotic analysis since $\hat{\sigma}_y$ only includes terms corresponding to integer eigenvalues (see, for example, (29)), and $\hat{w}$ only includes terms corresponding to noninteger eigenvalues (see, for example, (34)). However, (57) can be represented by (3) or (36) with nonvanishing coefficients $\alpha_1 = -0.2612$ and $\alpha_2 = -1.0215$, that is,

$$
\hat{\sigma}_y = 1 + \alpha_1 \hat{w}^{\frac{2}{3}} + \alpha_2 \hat{w}^{\frac{4}{3}} - (1 + \alpha_1 + \alpha_2)\hat{w}^2.
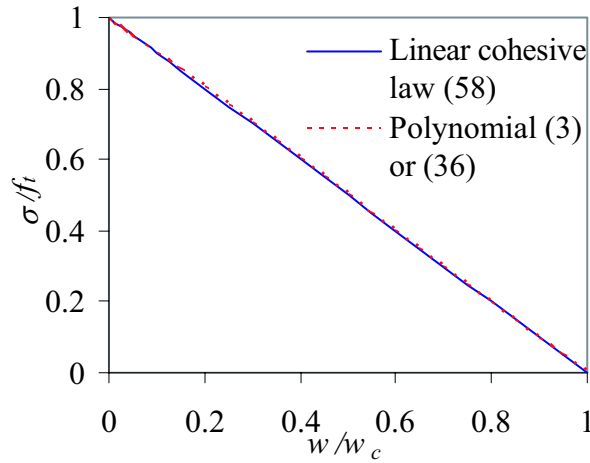$$

Figure 4. Linear tension-softening law.

The correlation coefficient is 1. The linear law Equation (57) is compared with Equation (3) in Figure 4; they cannot be distinguished on the scale of the figure. Hence results obtained in Section 4 can be used directly to the linear tension-softening law.

Similarly, the widely used bilinear tension-softening law (Figure 5)

$$
\hat{\sigma} = \begin{cases} 1 - (1 - \hat{f}_1)\dfrac{\hat{w}}{\hat{w}_1}, & 0 \le \hat{\sigma} \le \hat{f}_1 \\[2ex] \dfrac{\hat{f}_1}{1 - \hat{w}_1}(1 - \hat{w}), & \hat{f}_1 < \hat{\sigma} \le 1, \end{cases} \tag{58}
$$

(where $\hat{f}_1 = f_1/f_t$ and $\hat{w}_1 = w_1/w_c$) is also not suitable for the asymptotic analysis in Section 4.
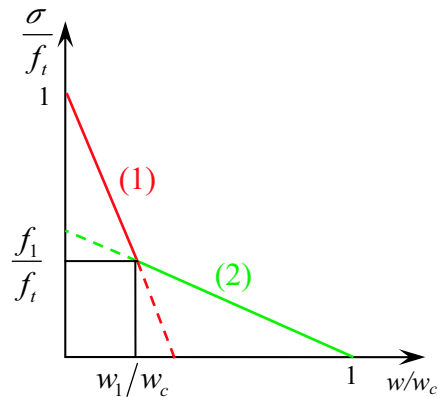
Figure 5. Bilinear tension-softening law.

However, its two linear parts Equations (1) and (2) can be rewritten into two linear laws as shown in 5. The first part can be written into (57) using a new definition of w_c as

$$w_c = \frac{w_1}{1 - \hat{f}_1}. \tag{59}$$

The second part can be written into (57) using a new definition of f_t as

$$f_t = \frac{f_1}{1 - \hat{w}_1}. \tag{60}$$

Then the asymptotic field of the bilinear law can be obtained by the corresponding linear cohesive laws.

Moreover, the procedures are also applicable to cohesion-separation relations in which the power of $\hat{w}$ is $2i$ rather than $2i/3$ as in Equation (3) or (36)

$$\hat{\sigma}_y = 1 + \sum_{i=1}^{5} \alpha_i \hat{w}^{2i} - \left(1 + \sum_{i=1}^{5} \alpha_i\right) \hat{w}^{12}. \tag{61}$$

For this relation, the counterpart of (38) becomes

$$\hat{w}^{2i} = d_0^{2i} r^{3i} \left(1 + \sum_{n=1}^{N} \beta_{in} r^n\right), \tag{62}$$

where

$$\beta_{in} = \frac{f_i^{(n)}(0)}{n!}, \qquad f_i(r) = \left(1 + \sum_{n=1}^{N} d_n r^n\right)^{2i}. \tag{63}$$

Substitution of Equation (62) into the right hand side of (61) gives

$$1 + \sum_{i=1}^{5} \alpha_i d_0^{2i} r^{3i} \left(1 + \sum_{n=1}^{N} \beta_{in} r^n\right) - \left(1 + \sum_{i=1}^{5} \alpha_i\right) d_0^{12} r^{18} \left(1 + \sum_{n=1}^{N} \beta_{6n} r^n\right).$$

Collecting the terms with like powers of r and comparing them with (29) results in relationships between the coefficients similar to (41).

Wecharatana [1990] introduced the softening relationship

$$\hat{\sigma}^m + \hat{w}^{2m} = 1 \tag{64}$$

(where $m = 0.27$ for concrete with compressive strength $f_c = 24\,\text{MPa}$ and $m = 0.2$ for concrete with $f_c = 83\,\text{MPa}$) to fit his experimental results from uniaxial tests on normal and high strength concrete using dog-bone-shaped specimens with edge notches (see also [Karihaloo 1995]). This relationship cannot be used in the asymptotic analysis above as m is not an integer. However, for $m = 0.27$ in the range of $0 \le \hat{w} \le 0.6$, we can fit Equation (64) using (3) or (36) with $\alpha_1 = -6.9495$, $\alpha_2 = 29.9794$, $\alpha_3 = -87.2663$, $\alpha_4 = 148.3647$, and $\alpha_5 = -128.84$. The correlation coefficient is 1. When $\hat{w} = 0.6$, then $\hat{\sigma} = 0.005148$; when $\hat{w} > 0.6$, then $\hat{\sigma}$ is negligibly small. As compared in Figure 6, they cannot be distinguished on the scale of the figure.
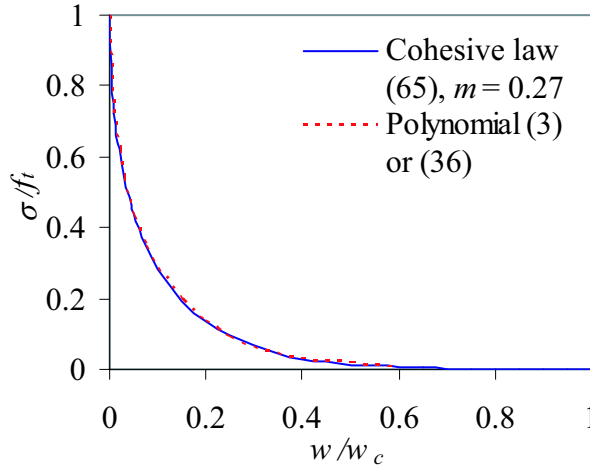
Figure 6. A comparison of cohesive law Equation (64) ($m = 0.27$) with polynomial Equation (3) or (36).

For $m = 0.2$ in the range of $0 \leq \hat{w} \leq 0.3$, Equation (64) can also be fitted using a polynomial in the form of (36) but including three higher order terms

$$\hat{\sigma}_y = 1 + \sum_{i=1}^{8} \alpha_i \hat{w}^{2/3i} - \left(1 + \sum_{i=1}^{8} \alpha_i\right)\hat{w}^6, \tag{65}$$

with

$$\alpha_1 = -25.77925, \qquad \alpha_2 = 459.7579,$$
$$\alpha_3 = -5.14083 \times 10^3, \qquad \alpha_4 = 3.51282 \times 10^4,$$
$$\alpha_5 = -1.48405 \times 10^5, \qquad \alpha_6 = 3.86621 \times 10^5,$$
$$\alpha_7 = -5.99122 \times 10^5, \qquad \alpha_8 = 4.99809 \times 10^5.$$

The correlation coefficient is also 1. When $\hat{w} = 0.3$, then $\hat{\sigma} = 0.008155$; when $\hat{w} > 0.3$, then $\hat{\sigma}$ is negligibly small. They are compared in Figure 7, and cannot be distinguished on the scale of the figure.

The simplest rectangular cohesive law in which the cohesive stress is constant and identical to the strength of the material f_t in the cohesive zone has also been used by some researchers. This law can be approximated by

$$\hat{\sigma}_y = 1 - \hat{w}^{2n} \tag{66}$$

as illustrated in Figure 8. Obviously, the cohesive law Equation (66) is a simplified form of (61) with coefficients $\alpha_i = 0$. The procedures and results for the cohesive law (61) are therefore correct for the rectangular law. Alternatively, the rectangular law can be enforced directly by assuming $\hat{\sigma}_y$ in (29) to be a constant, that is, all coefficients c_n $(n > 0)$ vanish and there are no further constraints on the coefficients.
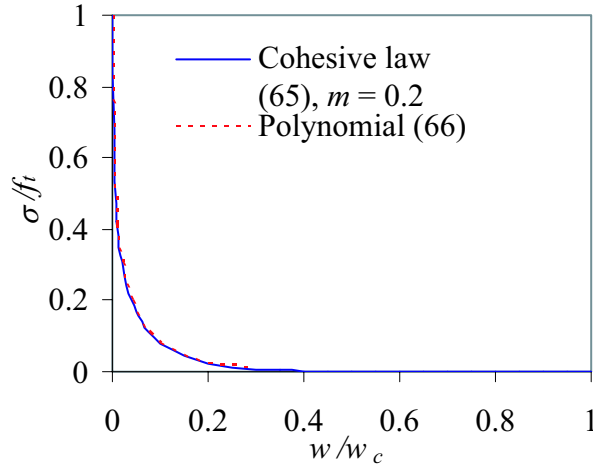
Figure 7. A comparison of the cohesive law Equation (64) ($m = 0.2$) with polynomial (65).
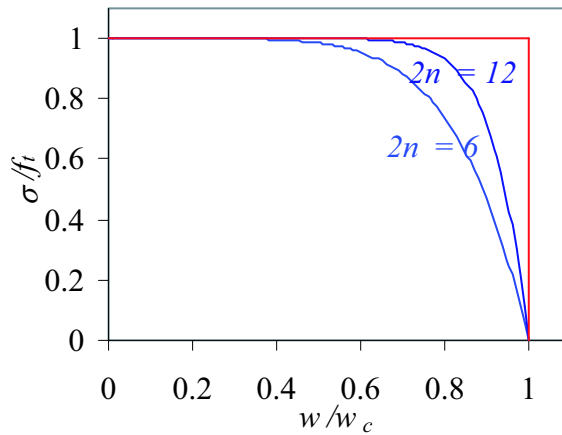
Figure 8. Comparison of the rectangular cohesive law with (66).

6. Implementation of the asymptotic fields in XFEM/GFEM and examples of mode I cohesive crack tip fields

In the context of the implementation of the cohesive crack asymptotic fields as enrichment functions in the XFEM/GFEM, if not only the first term but also the higher order terms are used as in [Liu et al. 2004], the linear dependence of the coefficients can be enforced in advance, while the nonlinear dependence of the coefficients can be enforced as constraints in the solution process. It is more convenient to use only the leading term of the displacement asymptotic field at the tip of a cohesive crack (which ensures a displacement discontinuity normal to the cohesive crack face) as the enrichment function, as in most implementations of the XFEM in the literature. The complete implementation with several examples can be found in [Xiao et al. 2006, in press].
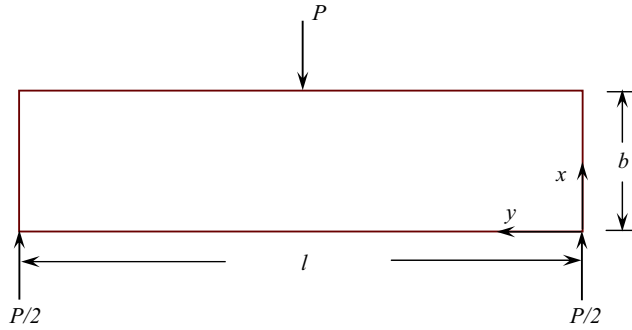
Figure 9. An unnotched three-point bend beam (TPB).

In the following, a typical mode I cohesive cracking problem of quasibrittle materials — a three point bend beam without any initial crack (Figure 9) made of a quasibrittle material with the linear softening law (57) — is analyzed. A state of plane strain is considered. The geometrical parameters are

$$b = 150\,\text{mm}, \qquad l = 4b, \qquad t = b,$$

where t is the specimen thickness in the out-of-plane direction. The material properties are

$$E = 36.5\,\text{GPa}, \qquad \nu = 0.1, \qquad f_t = 3.19\,\text{MPa}, \qquad G_F = 50\,\text{Nm}^{-1},$$

where E is Young's modulus, ν the Poisson ratio, and G_F the specific fracture energy. The dimensions for force and length are N and mm, respectively.

The details of simulation are the same as in [Xiao et al. 2006, in press]. Two meshes, as shown in Figure 10, are used in the analysis. The coarser mesh consists of $50 \times 100 = 5000$ rectangular elements, giving a total of 5151 nodes. The finer mesh consists of $150 \times 120 = 18000$ rectangular elements, giving a total of 18271 nodes. Both meshes are uniformly divided in the x-direction. For the coarser mesh, the central 50 layers of elements have an identical height (y-direction) of 3 mm; the remaining elements have an identical height of 9 mm. Therefore, elements in the central zone are $3 \times 3\,\text{mm}^2$ squares. For the finer mesh, the central 60 layers of elements have an identical height of 1 mm; the remaining elements have an identical height of 9 mm. Therefore elements in the central zone are $1 \times 1\,\text{mm}^2$ squares. The intention of using two meshes is to study the mesh size sensitivity of the global responses. The conventional 4-node bilinear isoparametric Q4 elements are also used as background elements. The first layer of nodes surrounding the cohesive crack tip (the elements that include the crack tip k are defined as the first layer elements of the crack tip with enriched nodes; the nodes in the first layer elements are called the first layer enriched nodes) are enriched with the first term of the asymptotic displacement field (50)–(54) at the tip of a cohesive crack corresponding to a noninteger eigenvalue that gives a normal displacement discontinuity over the cohesive-crack faces

$$u = \frac{r^{3/2}}{2\mu} a_{11}\left[\left(\kappa + \tfrac{1}{2}\right)\cos\tfrac{3}{2}\theta - \tfrac{3}{2}\cos\tfrac{1}{2}\theta\right], \tag{67}$$
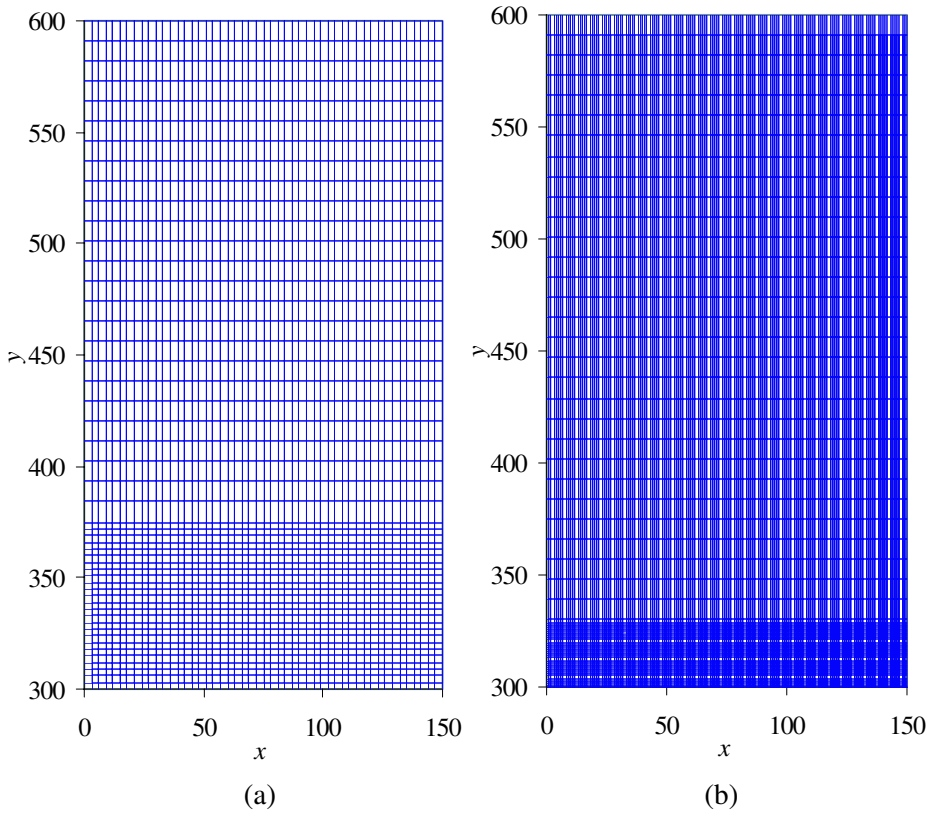
Figure 10. Coarse (a) and fine (b) mesh for half of the specimen.

$$v = \frac{r^{3/2}}{2\mu} a_{11}\left[\left(\kappa - \tfrac{1}{2}\right) \sin \tfrac{3}{2}\theta - \tfrac{3}{2} \sin \tfrac{1}{2}\theta\right]. \tag{68}$$

The potential fracture locus coincides with the specimen's axis of symmetry. The crack is modelled by enriching the nodes on the crack faces with jump and branch functions without the double nodes that are used in the traditional FEM.

As in [Moës and Belytschko 2002], the x-direction of nodes with coordinates $(0, 0)$ and $(0, 600\,\text{mm})$ and the y-direction of the node with coordinates $(150\,\text{mm}, 300\,\text{mm})$ are constrained; the load is distributed over a length of 6 mm in the coarse mesh (Figure 10a) and 2 mm (2 elements) in the fine mesh (10b). Since a low Poisson ratio of 0.1 is used, the results are believed to be close to those of Carpinteri and Colombo [1989], where a plane stress condition is assumed and a concentrated load was considered.

The nondimensional load-midspan deflection curves are shown in 11(a). They agree very well with the results of Carpinteri and Colombo [1989]. The evolution of the cohesive zone size as the cohesive tip travels through the beam is shown in Figure 11(b), which agrees very well with [Moës and Belytschko 2002]. It is clear that the results are insensitive to the mesh size.

In order to visualize the cohesive crack tip fields derived in Section 4, it is necessary to determine the unknown coefficients by fitting the numerically computed crack tip fields with the theoretically obtained fields. This requires a sophisticated optimization scheme. For the present purpose of illustration, we
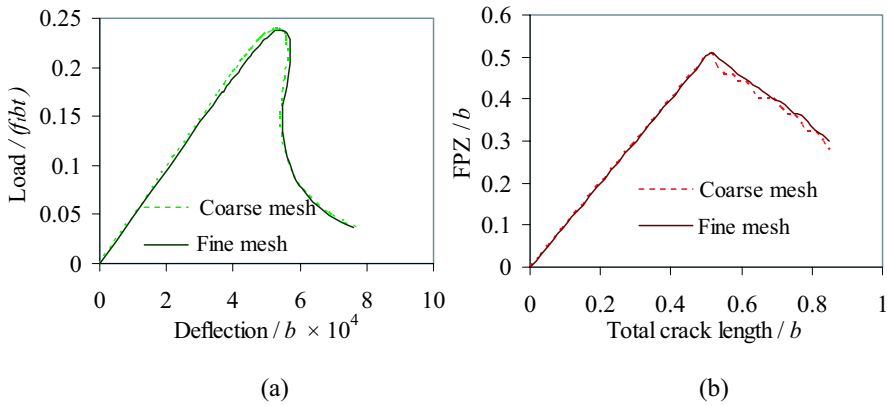
Figure 11. (a) Nondimensional load-midspan deflection curves of the three-point bend beam ($G_F = 50\,\mathrm{Nm}^{-1}$); (b) evolution of the cohesive zone size as the cohesive tip travels through the beam.

will solve a mode I cohesive crack problem shown in Figure 12 using the obtained asymptotic fields and the numerically computed opening profile of the cohesive crack. The dimensions of the displacement and length parameters are in millimeters and those of the stresses in megapascals, unless mentioned otherwise.

We consider the subdomain bounded by broken lines in Figure 12, and assume the length of the cohesive crack is 10.5 mm. The opening profile of the cohesive crack (Figure 13) adopts the computed results above at the loading stage with the total cohesive crack = 31.5 mm and load/($f_t bt$) = 0.228. It can be represented by the expansion Equation (55) corresponding to noninteger eigenvalues with nonvanishing coefficients

$$a_{10} = -0.192, \qquad a_{11} = -5.708 \cdot 10^{-3}, \qquad a_{12} = 1.2339 \cdot 10^{-5}.$$

From these coefficients, we can obtain parameters β Equation (40) and c (41). The cohesive stress (29) corresponding to these coefficients c is compared in Figure 14 with the results obtained by the linear tension-softening relationship Equation (57). The agreement is excellent, with a maximum error less than 0.5%.
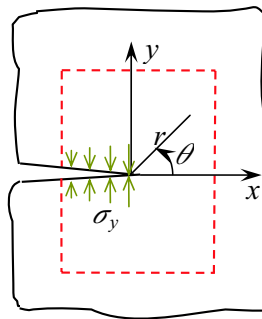
Figure 12. Illustration of the cohesive crack problem.
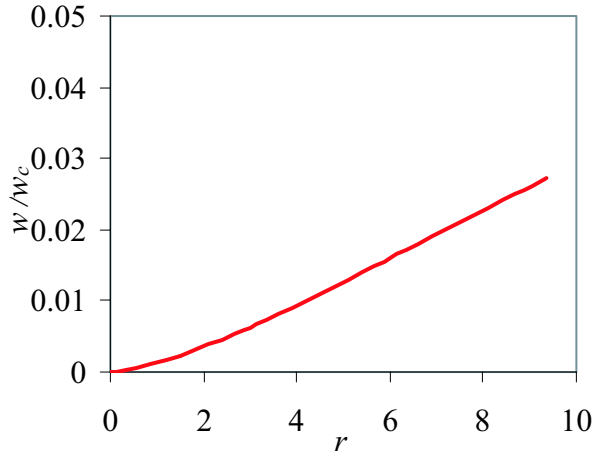
Figure 13. Opening profile of the cohesive crack.
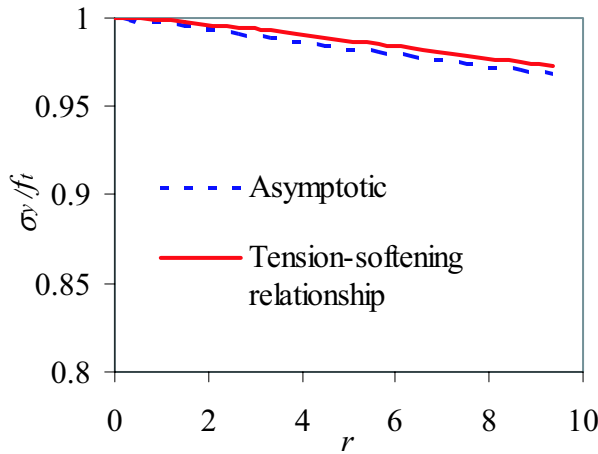
Figure 14. Comparison of the cohesive stress obtained by the tension-softening relationship Equation (57) and the asymptotic analysis.

The c coefficients also provide relationships between coefficients a_{1n} and b_{1n} for each integer eigenvalue as in Equation (30). In other words, the complete asymptotic fields are known except the coefficients a or b corresponding to integer eigenvalues. They are determined from the applied boundary conditions. Since we have assumed the crack opening profile, we cannot assume the prescribed boundary conditions again to avoid inconsistency. Therefore some weaker constraints are used instead.

We assume the boundary $x = -10.5$ is, or is very close to, a traction-free surface. Then the coefficients a_{1n} or b_{1n} for integer eigenvalues can be determined by assuming the boundary $x = -10.5$ to be nearly traction-free. More precisely, we divide the segment $x = -10.5$, $0 \le y \le 10.5$ into 100 identical segments, and minimize the value of σ_x and τ_{xy} at these 101 locations (including corner nodes) using the *Minimize* function of Mathcad 11. The convergence and constraint tolerances are chosen as 10^{-8}. The values
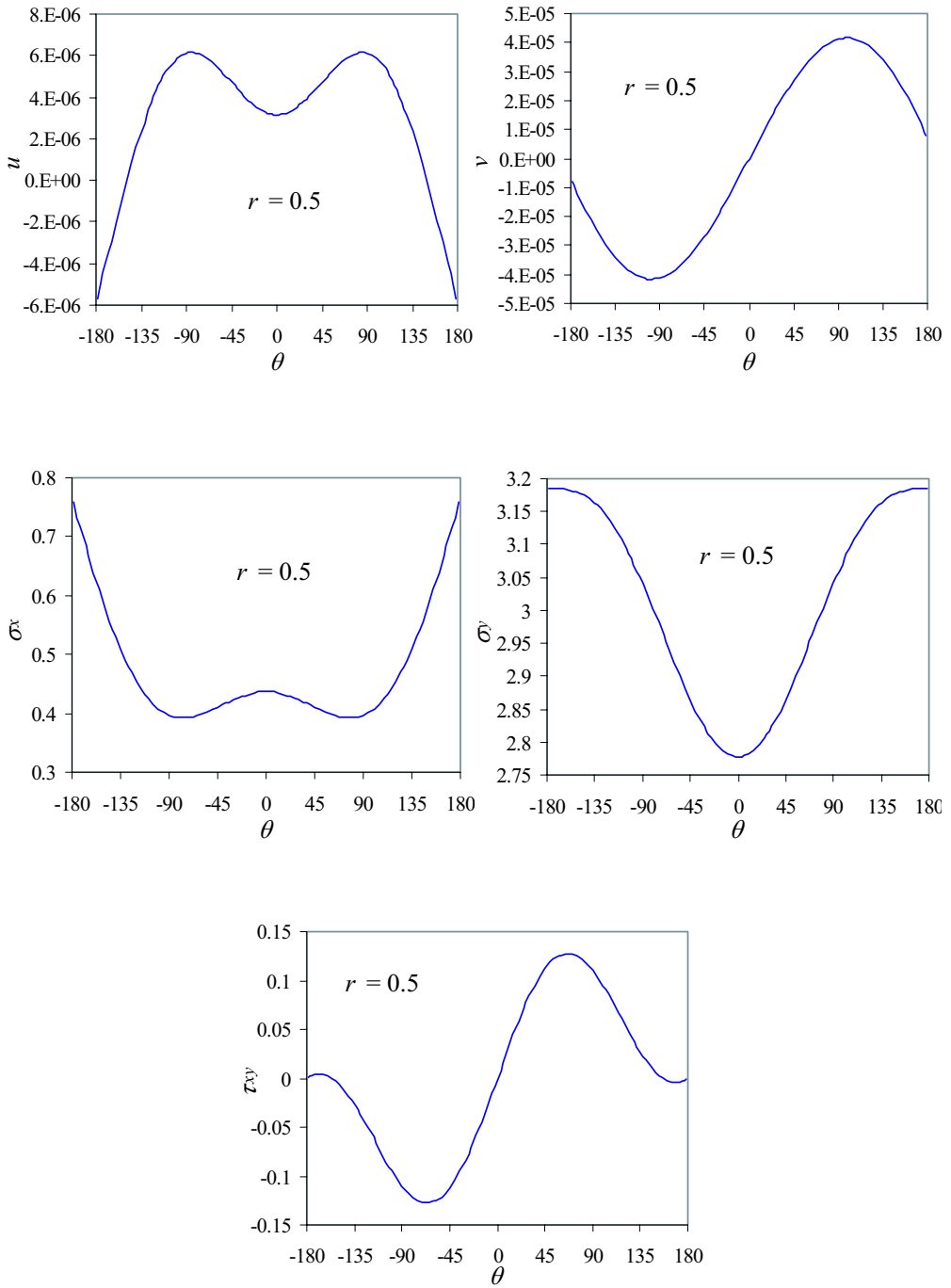
Figure 15. Displacements and stresses along the circle $r = 0.5$.
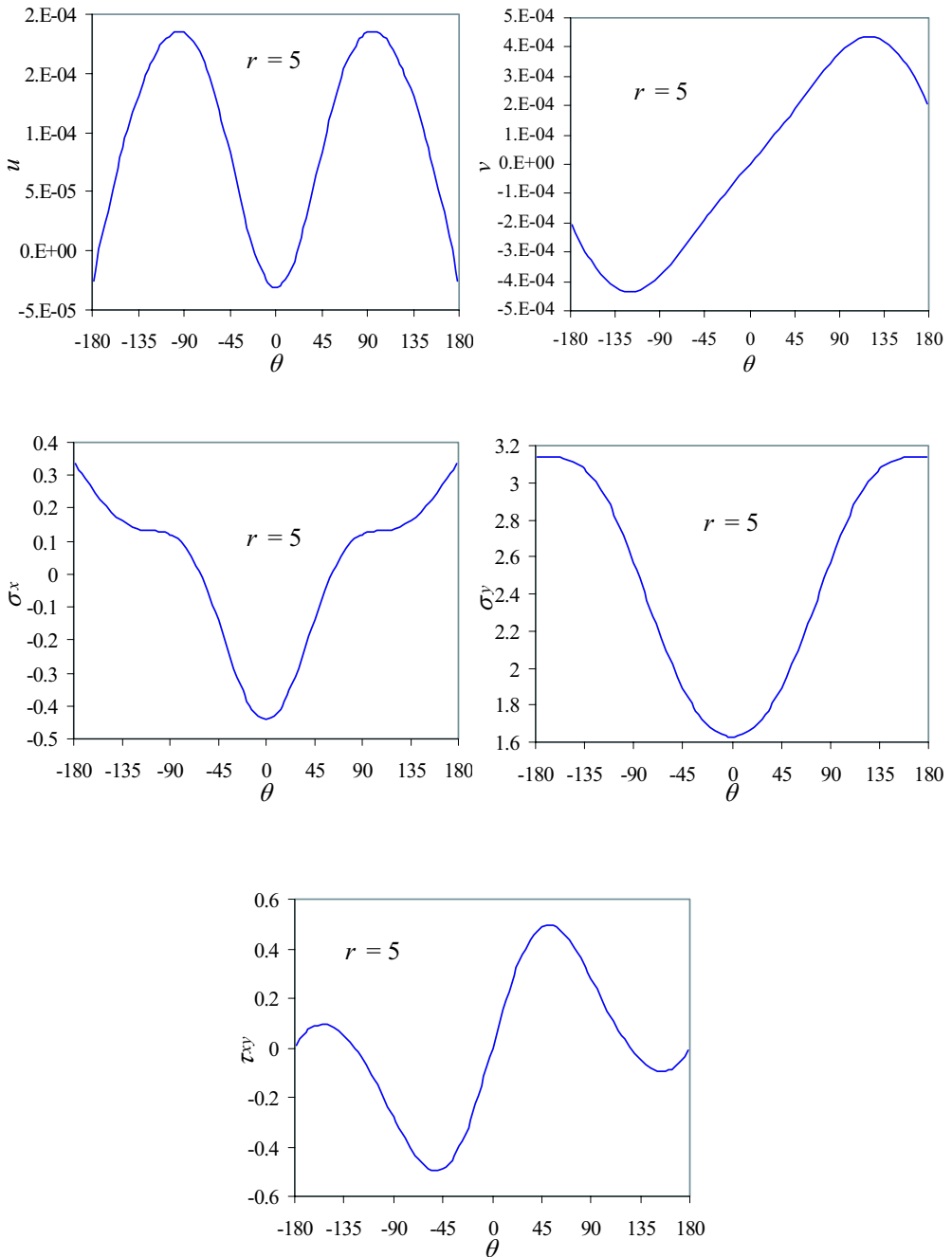
Figure 16. Displacements and stresses along the circle $r = 5$.
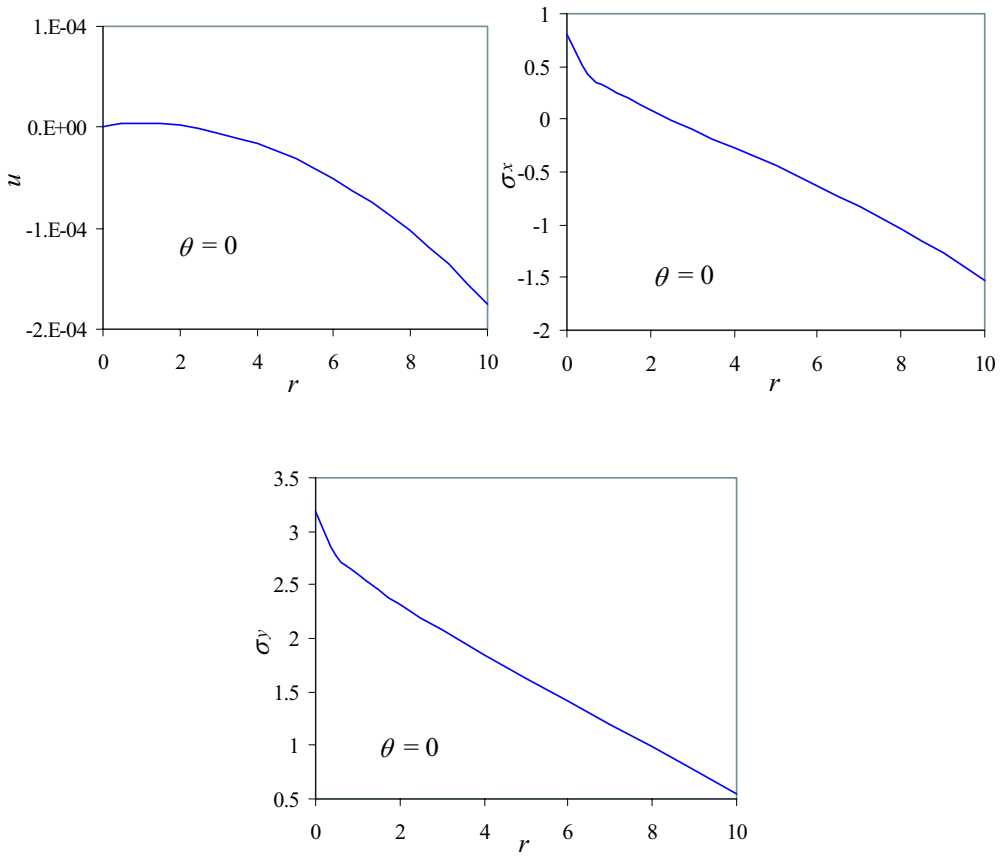
Figure 17. Nonvanishing displacements and stresses along the line of extension of the cohesive crack ($\theta = 0$).

$a_{10} = 1$, $a_{11} = 10^{-3}$, $a_{12} = -10^{-5}$, and $a_{13} = -10^{-5}$ are chosen as initial guesses. We obtain the coefficients for integer eigenvalues as

$$a_{10} = 0.9604, \quad a_{11} = 0.0124, \quad a_{12} = -2.1858 \cdot 10^{-4}, \quad a_{13} = -1.9741 \cdot 10^{-5},$$
$$b_{10} = 0.595, \quad b_{11} = -0.0107, \quad b_{12} = 1.9553 \cdot 10^{-4}, \quad b_{13} = 1.8647 \cdot 10^{-5},$$

with very small σ_x and τ_{xy} on the segment $x = -10.5$, $0 \leq y \leq 10.5$. Coefficients of the higher order terms are negligibly small.

The displacements and stresses corresponding to these coefficients along two circles surrounding the crack tip and the line of extension of the cohesive crack are plotted in Figures 15–17. Away from the crack tip, the distribution of the displacement and/or stress may be quite different. As expected, the stress σ_y at the cohesive crack tip is equal to f_t, and no stress at any other locations reaches f_t.

These solutions are exact when the displacements or tractions corresponding to them are applied on the boundary, as in the broken lines shown in Figure 12.

Near the cohesive crack tip, the maximum values of the main stresses σ_x and σ_y occur on the cohesive crack faces. This is because we have chosen the cohesive crack opening profile (Figure 13) corresponding to a TPB test. This feature of the stress distribution for this type of specimen has also been noticed by Planas et al. [2003] and validated by our own numerical analysis.

7. Conclusions and discussion

The asymptotic fields obtained in Section 4 are universal for the prescribed normal cohesion-separation relation. However, relationships Equation (41) between the coefficients are dependent on the softening relation of the material. The actual values of the coefficients are dependent on the geometry and boundary/loading conditions of the problem, as in the Williams expansion of a traction-free crack. The cohesive crack asymptotic fields obtained here can be used as enrichment functions in the extended/generalized finite element method at the tip of long cohesive cracks, as well as short branches/kinks.

In traction-free cracks, terms in Equations (19)–(23) corresponding to different eigenvalues are independent, that is, controlled by independent coefficients. In the cohesive crack tip fields some of the terms can be dependent and not controlled by independent coefficients. Such a dependence also exists in the higher order terms of the crack tip fields in elastoplastic power-law hardening materials (see [Xia et al. 1993; Yang et al. 1993; 1996; Chao and Yang 1996] and a review by Karihaloo and Xiao [2003a]).

In this paper, we have applied a complex-function formulation of homogeneous isotropic linear elasticity for simplicity; however, the derivation can be easily extended to bimaterial interfacial cracks (see [Rice 1988]) and/or anisotropic elasticity. Anisotropy can be treated with the Stroh formalism [Stroh 1958; Suo 1990; Deng 1994].

Appendix: Derivatives of $f_i(r)$

The first five derivatives of $f_i(r)$ in Equation (39) are

$$f_i^{(1)}(r) = \tfrac{2}{3}i\left(1 + \sum_{n=1}^{N} d_n r^n\right)^{\frac{2}{3}i-1} \sum_{n=1}^{N} d_n n r^{n-1};$$

$$f_i^{(2)}(r) = \tfrac{2}{3}i\left(\tfrac{2}{3}i - 1\right)\left(1 + \sum_{n=1}^{N} d_n r^n\right)^{\frac{2}{3}i-2}\left(\sum_{n=1}^{N} d_n n r^{n-1}\right)^2 + \tfrac{2}{3}i\left(1 + \sum_{n=1}^{N} d_n r^n\right)^{\frac{2}{3}i-1} \sum_{n=2}^{N} d_n n(n-1) r^{n-2};$$

$$\begin{aligned}
f_i^{(3)}(r) = {} & \tfrac{2}{3}i\left(\tfrac{2}{3}i - 1\right)\left(\tfrac{2}{3}i - 2\right)\left(1 + \sum_{n=1}^{N} d_n r^n\right)^{\frac{2}{3}i-3}\left(\sum_{n=1}^{N} d_n n r^{n-1}\right)^3 \\
& + \tfrac{6}{3}i\left(\tfrac{2}{3}i - 1\right)\left(1 + \sum_{n=1}^{N} d_n r^n\right)^{\frac{2}{3}i-2} \sum_{n=1}^{N} d_n n r^{n-1} \sum_{n=2}^{N} d_n n(n-1) r^{n-2} \\
& + \tfrac{2}{3}i\left(1 + \sum_{n=1}^{N} d_n r^n\right)^{\frac{2}{3}i-1} \sum_{n=3}^{N} d_n n(n-1)(n-2) r^{n-3};
\end{aligned}$$

$$f_i^{(4)}(r) = \tfrac{2}{3}i\left(\tfrac{2}{3}i-1\right)\left(\tfrac{2}{3}i-2\right)\left(\tfrac{2}{3}i-3\right)\left(1+\sum_{n=1}^{N}d_n r^n\right)^{\frac{2}{3}i-4}\left(\sum_{n=1}^{N}d_n n r^{n-1}\right)^4$$

$$+\tfrac{12}{3}i\left(\tfrac{2}{3}i-1\right)\left(\tfrac{2}{3}i-2\right)\left(1+\sum_{n=1}^{N}d_n r^n\right)^{\frac{2}{3}i-3}\left(\sum_{n=1}^{N}d_n n r^{n-1}\right)^2\sum_{n=2}^{N}d_n n(n-1)r^{n-2}$$

$$+\tfrac{6}{3}i\left(\tfrac{2}{3}i-1\right)\left(1+\sum_{n=1}^{N}d_n r^n\right)^{\frac{2}{3}i-2}\left(\sum_{n=2}^{N}d_n n(n-1)r^{n-2}\right)^2$$

$$+\tfrac{8}{3}i\left(\tfrac{2}{3}i-1\right)\left(1+\sum_{n=1}^{N}d_n r^n\right)^{\frac{2}{3}i-2}\sum_{n=1}^{N}d_n n r^{n-1}\sum_{n=3}^{N}d_n n(n-1)(n-2)r^{n-3}$$

$$+\tfrac{2}{3}i\left(1+\sum_{n=1}^{N}d_n r^n\right)^{\frac{2}{3}i-1}\sum_{n=4}^{N}d_n n(n-1)(n-2)(n-3)r^{n-4};$$

$$f_i^{(5)}(r) = \tfrac{2}{3}i\left(\tfrac{2}{3}i-1\right)\left(\tfrac{2}{3}i-2\right)\left(\tfrac{2}{3}i-3\right)\left(\tfrac{2}{3}i-4\right)\times\left(1+\sum_{n=1}^{N}d_n r^n\right)^{\frac{2}{3}i-5}\left(\sum_{n=1}^{N}d_n n r^{n-1}\right)^5$$

$$+\tfrac{20}{3}i\left(\tfrac{2}{3}i-1\right)\left(\tfrac{2}{3}i-2\right)\left(\tfrac{2}{3}i-3\right)\left(1+\sum_{n=1}^{N}d_n r^n\right)^{\frac{2}{3}i-4}\times\left(\sum_{n=1}^{N}d_n n r^{n-1}\right)^3\sum_{n=2}^{N}d_n n(n-1)r^{n-2}$$

$$+\tfrac{30}{3}i\left(\tfrac{2}{3}i-1\right)\left(\tfrac{2}{3}i-2\right)\left(1+\sum_{n=1}^{N}d_n r^n\right)^{\frac{2}{3}i-3}\sum_{n=1}^{N}d_n n r^{n-1}\left(\sum_{n=2}^{N}d_n n(n-1)r^{n-2}\right)^2$$

$$+\tfrac{20}{3}i\left(\tfrac{2}{3}i-1\right)\left(\tfrac{2}{3}i-2\right)\left(1+\sum_{n=1}^{N}d_n r^n\right)^{\frac{2}{3}i-3}\left(\sum_{n=1}^{N}d_n n r^{n-1}\right)^2\times\sum_{n=3}^{N}d_n n(n-1)(n-2)r^{n-3}$$

$$+\tfrac{20}{3}i\left(\tfrac{2}{3}i-1\right)\left(1+\sum_{n=1}^{N}d_n r^n\right)^{\frac{2}{3}i-2}\sum_{n=2}^{N}d_n n(n-1)r^{n-2}\sum_{n=3}^{N}d_n n(n-1)(n-2)r^{n-3}$$

$$+\tfrac{10}{3}i\left(\tfrac{2}{3}i-1\right)\left(1+\sum_{n=1}^{N}d_n r^n\right)^{\frac{2}{3}i-2}\sum_{n=1}^{N}d_n n r^{n-1}\sum_{n=4}^{N}d_n n(n-1)(n-2)(n-3)r^{n-4}$$

$$+\tfrac{2}{3}i\left(1+\sum_{n=1}^{N}d_n r^n\right)^{\frac{2}{3}i-1}\sum_{n=5}^{N}d_n n(n-1)(n-2)(n-3)(n-4)r^{n-5}.$$

Acknowledgment

References

[Abdalla and Karihaloo 2004] H. M. Abdalla and B. L. Karihaloo, "A method for constructing the bilinear tension softening diagram of concrete corresponding to its true fracture energy", *Mag. Concr. Res.* **56**:10 (2004), 597–604.

[Babuška et al. 2003] I. Babuška, U. Banerjee, and J. E. Osborn, "Survey of meshless and generalized finite element methods: A unified approach", *Acta Numerica* **12** (2003), 1–125.

[Barenblatt 1962] G. I. Barenblatt, "The mathematical theory of equilibrium cracks in brittle fracture", *Adv. Appl. Mech.* **7** (1962), 55–129.

[Bialas and Mróz 2005] M. Bialas and Z. Mróz, "Modelling of progressive interface failure under combined normal compression and shear stress", *Int. J. Solids Struct.* **42**:15 (2005), 4436–4467.

[de Borst et al. 2004] R. de Borst, M. A. Gutierrez, G. N. Wells, J. J. C. Remmers, and H. Askes, "Cohesive-zone models, higher-order continuum theories and reliability methods for computational failure analysis", *Int. J. Numer. Methods Eng.* **60**:1 (2004), 289–315.

[Carpinteri and Colombo 1989] A. Carpinteri and G. Colombo, "Numerical analysis of catastrophic softening behaviour (snap-back instability)", *Comput. Struct.* **31**:4 (1989), 607–636.

[Chandra et al. 2002] N. Chandra, H. Li, C. Shet, and H. Ghonem, "Some issues in the application of cohesive zone models for metal-ceramic interfaces", *Int. J. Solids Struct.* **39**:10 (2002), 2827–2855.

[Chao and Yang 1996] Y. J. Chao and S. Yang, "Higher order crack tip fields and its implication for fracture of solids under mode II conditions", *Eng. Fract. Mech.* **55**:5 (1996), 777–794.

[Cocchetti et al. 2002] G. Cocchetti, G. Maier, and X. P. Shen, "Piecewise linear models for interfaces and mixed mode cohesive cracks", *Comput. Model. Eng. Sci.* **3**:3 (2002), 279–298.

[Cornelissen et al. 1986] H. A. W. Cornelissen, D. A. Hordijk, and H. W. Reinhardt, "Experimental determination of crack softening characteristics of normalweight and lightweight concrete", *Heron* **31**:2 (1986), 45–56.

[Deng 1994] X. M. Deng, "An asymptotic analysis of stationary and moving cracks with frictional contact along bimaterial interfaces and in homogeneous solids", *Int. J. Solids Struct.* **31**:17 (1994), 2407–2429.

[Dugdale 1960] D. S. Dugdale, "Yielding of steel sheets containing slits", *J. Mech. Phys. Solids* **8**:2 (1960), 100–104.

[Elices et al. 2002] M. Elices, G. V. Guinea, J. Gómez, and J. Planas, "The cohesive zone model: advantages, limitations and challenges", *Eng. Fract. Mech.* **69**:2 (2002), 137–163.

[Hansbo and Hansbo 2004] A. Hansbo and P. Hansbo, "A finite element method for the simulation of strong and weak discontinuities in solid mechanics", *Comput. Methods Appl. Mech. Eng.* **193**:33–35 (2004), 3523–3540.

[Hillerborg et al. 1976] A. Hillerborg, M. Modéer, and P. E. Petersson, "Analysis of crack formation and crack growth in concrete by means of fracture mechanics and finite elements", *Cem. Concr. Res.* **6**:6 (1976), 773–782.

[Hong and Kim 2003] S. S. Hong and K. S. Kim, "Extraction of cohesive-zone laws from elastic far-fields of a cohesive crack tip: a field projection method", *J. Mech. Phys. Solids* **51**:7 (2003), 1267–1286.

[Hutchinson and Evans 2000] J. W. Hutchinson and A. G. Evans, "Mechanics of materials: top-down approaches to fracture", *Acta Mater.* **48**:1 (2000), 125–135.

[Karihaloo 1995] B. L. Karihaloo, *Fracture mechanics and structural concrete*, Addison Wesley Longman, UK, 1995.

[Karihaloo 1999] B. L. Karihaloo, "Size effect in shallow and deep notched quasi-brittle structures", *Int. J. Fract.* **95**:1-4 (1999), 379–390.

[Karihaloo and Xiao 2003a] B. L. Karihaloo and Q. Z. Xiao, "Linear and nonlinear fracture mechanics", pp. 81–212 in *Comprehensive structural integrity, II: fundamental theories and mechanisms of failure*, vol. 2, edited by B. L. Karihaloo and W. G. Knauss, Elsevier Pergamon, UK, 2003.

[Karihaloo and Xiao 2003b] B. L. Karihaloo and Q. Z. Xiao, "Modelling of stationary and growing cracks in FE framework without remeshing: a state-of-the-art review", *Comput. Struct.* **81**:3 (2003), 119–129.

[Karihaloo et al. 2003] B. L. Karihaloo, H. M. Abdalla, and T. Imjai, "A simple method for determining the true specific fracture energy of concrete", *Mag. Concr. Res.* **55**:5 (2003), 471–481.

[Leblond and Frelat 2004] J. B. Leblond and J. L. Frelat, "Crack kinking from an initially closed, ordinary or interface crack, in the presence of friction", *Eng. Fract. Mech.* **71**:3 (2004), 289–307.

[Liu et al. 2004] X. Y. Liu, Q. Z. Xiao, and B. L. Karihaloo, "XFEM for direct evaluation of mixed mode SIFs in homogeneous and bi-materials", *Int. J. Numer. Methods Eng.* **59**:8 (2004), 1103–1118.

[Moës and Belytschko 2002] N. Moës and T. Belytschko, "Extended finite element method for cohesive crack growth", *Eng. Fract. Mech.* **69**:7 (2002), 813–833.

[Moës et al. 1999] N. Moës, J. Dolbow, and T. Belytschko, "A finite element method for crack growth without remeshing", *Int. J. Numer. Methods Eng.* **46**:1 (1999), 131–150.

[Mróz and Bialas 2005] Z. Mróz and M. Bialas, "A simplified analysis of interface failure under compressive normal stress and monotonic or cyclic shear loading", *Int. J. Numer. Anal. Methods Geomech.* **29**:4 (2005), 337–368.

[Muskhelishvili 1953] N. I. Muskhelishvili, *Some basic problems of mathematical theory of elasticity*, Noordhoff, Holland, 1953.

[Owen and Fawkes 1983] D. R. J. Owen and A. J. Fawkes, *Engineering fracture mechanics: numerical methods and applications*, Pineridge Press Ltd., Swansea, UK, 1983.

[Planas et al. 2001] J. Planas, Z. P. Bazant, and M. Jirasek, "Reinterpretation of Karihaloo's size effect analysis for notched quasibrittle structures", *Int. J. Fract.* **111**:1 (2001), 17–28.

[Planas et al. 2003] J. Planas, M. Elices, G. V. Guinea, F. J. Gómez, D. A. Cendón, and I. Arbilla, "Generalizations and specializations of cohesive crack models", *Eng. Fract. Mech.* **70**:14 (2003), 1759–1776.

[Remmers et al. 2003] J. J. C. Remmers, R. de Borst, and A. Needleman, "A cohesive segments method for the simulation of crack growth", *Comput. Mech.* **31**:1-2 (2003), 69–77.

[Rice 1988] J. R. Rice, "Elastic fracture mechanics concepts for interfacial cracks", *J. Appl. Mech. (Trans. ASME)* **55** (1988), 98–103.

[Sih and Liebowitz 1968] G. C. Sih and H. Liebowitz, *Mathematical theories of brittle fracture*, vol. II, Chapter Fracture: an advanced treatise, pp. 67–190, Academic Press, New York, 1968.

[Stroh 1958] A. N. Stroh, "Dislocations and cracks in anisotropic elasticity", *Philos. Mag. (8)* **3** (1958), 625–646.

[Strouboulis et al. 2001] T. Strouboulis, K. Copps, and I. Babuška, "The generalized finite element method", *Comput. Methods Appl. Mech. Eng.* **190**:32–33 (2001), 4081–4193.

[Suo 1990] Z. Suo, "Singularities, interfaces and cracks in dissimilar anisotropic media", *Proc. Roy. Soc. London Ser. A* **427**:1873 (1990), 331–358.

[Valente 1991] S. Valente, "Influence of friction on cohesive crack-propagation", pp. 695–704 in *Fracture processes in concrete, rock and ceramics*, edited by J. G. M. van Mier et al., RILEM Proceedings **13**, London, 1991.

[Wecharatana 1990] M. Wecharatana, "Brittleness index of cementitious composite", in *Serviceability and durability of construction materials*, edited by B. A. Suprenant, ASCE Publications, New York, 1990.

[Wells and Sluys 2001] G. N. Wells and L. J. Sluys, "A new method for modeling cohesive cracks using finite elements", *Int. J. Numer. Methods Eng.* **50**:12 (2001), 2667–2682.

[Williams 1957] M. L. Williams, "On the stress distribution at the base of a stationary crack", *J. Appl. Mech. (Trans. ASME)* **24** (1957), 109–114.

[Xia et al. 1993] L. Xia, T. C. Wang, and C. F. Shih, "Higher-order analysis of crack tip fields in elastic power-law hardening materials", *J. Mech. Phys. Solids* **41**:4 (1993), 665–687.

[Xiao and Karihaloo 2005] Q. Z. Xiao and B. L. Karihaloo, "Recent developments of the extended/generalized FEM and a comparison with the FEM", pp. 303–324 in *Developments and applications of solid mechanics, Proceedings of the Symposium for Professor M. G. Huang's 90th Birthday*, edited by X. P. Wu, Press of University of Science and Technology of China, China, 2005.

[Xiao et al. 2006, in press] Q. Z. Xiao, B. L. Karihaloo, and X. Y. Liu, "Incremental-secant modulus iteration scheme and stress recovery for simulating cracking process in quasi-brittle materials using XFEM", *Int. J. Numer. Mech. Eng.* (2006, in press).

[Yang et al. 1993] S. Yang, Y. J. Chao, and M. A. Sutton, "Higher order asymptotic crack tip fields in a power-law hardening material", *Eng. Fract. Mech.* **45**:1 (1993), 1–20.

[Yang et al. 1996] S. Yang, F. G. Yuan, and X. Cai, "Higher order asymptotic elastic-plastic crack-tip fields under antiplane shear", *Eng. Fract. Mech.* **54**:3 (1996), 405–422.

QIZHI XIAO: xiaoq@cardiff.ac.uk
School of Engineering, Cardiff University, Queen's Buildings, The Parade, Cardiff CF24 3AA, United Kingdom

BHUSHAN LAL KARIHALOO: karihaloob@cardiff.ac.uk
School of Engineering, Cardiff University, Queen's Buildings, The Parade, Cardiff CF24 3AA, United Kingdom

JOURNAL OF MECHANICS OF MATERIALS AND STRUCTURES

Journal of Mechanics of Materials and Structures

Volume 1, Nº 5   May 2006